The Plant Cell, Vol. 28: 2026–2042, September 2016, www.plantcell.org

BREAKTHROUGH REPORT

Synergism between Inositol Polyphosphates and TOR Kinase Signaling in Nutrient Sensing, Growth Control, and Lipid Metabolism in Chlamydomonas[OPEN]

Inmaculada Couso,[a,1] Bradley S. Evans,[a] Jia Li,[a] Yu Liu,[a] Fangfang Ma,[a,2] Spencer Diamond,[b,3] Doug K. Allen,[a,c] and James G. Umen[a,4]

[a] Donald Danforth Plant Science Center, St. Louis, Missouri 63132
[b] Earth and Planetary Science, University of California, Berkeley, California 94720
[c] Agricultural Research Service, U.S. Department of Agriculture, St. Louis, Missouri 63132

ORCID IDs: 0000-0003-2849-675X (I.C.); 0000-0001-7220-0675 (F.M.); 0000-0001-8599-8946 (D.K.A.); 0000-0003-4094-9045 (J.G.U.)

The networks that govern carbon metabolism and control intracellular carbon partitioning in photosynthetic cells are poorly understood. Target of Rapamycin (TOR) kinase is a conserved growth regulator that integrates nutrient signals and modulates cell growth in eukaryotes, though the TOR signaling pathway in plants and algae has yet to be completely elucidated. We screened the unicellular green alga *Chlamydomonas reinhardtii* using insertional mutagenesis to find mutants that conferred hypersensitivity to the TOR inhibitor rapamycin. We characterized one mutant, *vip1-1*, that is predicted to encode a conserved inositol hexakisphosphate kinase from the VIP family that pyrophosphorylates phytic acid ($InsP_6$) to produce the low abundance signaling molecules $InsP_7$ and $InsP_8$. Unexpectedly, the rapamycin hypersensitive growth arrest of *vip1-1* cells was dependent on the presence of external acetate, which normally has a growth-stimulatory effect on Chlamydomonas. *vip1-1* mutants also constitutively overaccumulated triacylglycerols (TAGs) in a manner that was synergistic with other TAG inducing stimuli such as starvation. *vip1-1* cells had reduced $InsP_7$ and $InsP_8$, both of which are dynamically modulated in wild-type cells by TOR kinase activity and the presence of acetate. Our data uncover an interaction between the TOR kinase and inositol polyphosphate signaling systems that we propose governs carbon metabolism and intracellular pathways that lead to storage lipid accumulation.

INTRODUCTION

Photosynthetic cells are defined by their ability to fix and metabolize inorganic carbon (CO_2 or HCO_3^-). Many photosynthetic organisms can also grow heterotrophically or mixotrophically using externally supplied organic carbon or with a combination of photosynthesis and imported organic carbon (Pringsheim and Wiessner, 1960; Koch, 2004; Harris, 2009a; Morales-Sánchez et al., 2015). The means by which photosynthetic cells coordinate these two modes of carbon metabolism are relatively unexplored (Sheen, 1994; Coruzzi and Bush, 2001; Halford and Paul, 2003; Smith and Stitt, 2007), but the elucidation of intracellular carbon regulatory networks has the potential to improve our understanding of photosynthetic cell growth and provide insights that will allow harnessing of photosynthesis for improved yields and storage of fixed carbon.

The unicellular green alga *Chlamydomonas reinhardtii* is a model organism that has been used successfully to dissect and understand photosynthetic metabolism (Rochaix, 1995; Grossman, 2000; Dent et al., 2005; Minagawa and Tokutsu, 2015; Goodenough, 2015). Chlamydomonas cells can grow phototrophically and can also metabolize acetate and related compounds to grow mixotrophically or heterotrophically. The relationship between these modes of growth is complex and involves partial suppression of photosynthesis and alterations in gene expression when acetate is present (Heifetz et al., 2000; Boyle and Morgan, 2009; Johnson and Alric, 2012; Roach et al., 2013; Chapman et al., 2015). However, very little is known about intracellular signaling pathways that sense carbon source and control carbon metabolism and utilization in Chlamydomonas.

Target of Rapamycin (TOR) protein kinase is a conserved and essential regulator of eukaryotic cell growth that is thought to integrate external and internal metabolic cues to balance cell growth with energy and nutrient supplies (Menand et al., 2002; Loewith and Hall, 2011; Montané and Menand, 2013; Xiong and Sheen, 2012; Xiong et al., 2013; Rexin et al., 2015). In yeast and metazoans, TOR is found in two different complexes, TORC1 and TORC2, with distinct functions in cell growth and cytoskeletal organization, respectively, while green algae and land plants only

[1] Current Address: Instituto de Bioquímica Vegetal y Fotosíntesis, Seville 41092, Spain.
[2] Current Address: University of Florida, Gainesville, FL 32611.
[3] Current Address: Earth and Planetary Science, University of California, Berkeley, CA 94720-4767.
[4] Address correspondence to jumen@danforthcenter.org.
The author responsible for distribution of materials integral to the findings presented in this article in accordance with the policy described in the Instructions for Authors (www.plantcell.org) is: James G. Umen (jumen@danforthcenter.org).
[OPEN]Articles can be viewed without a subscription.
www.plantcell.org/cgi/doi/10.1105/tpc.16.00351

contain the components of TORC1, namely, TOR, RAPTOR, and LST8 (Díaz-Troya et al., 2008; Loewith and Hall, 2011; Moreau et al., 2012; Maegawa et al., 2015). In plants, the TOR complex plays similar roles as TORC1 in animals and fungi by influencing cytoplasmic protein translation, carbon metabolism, cell growth, cell proliferation, senescence, and autophagy (Deprost et al., 2007; Liu and Bassham, 2010; Caldana et al., 2013; Xiong and Sheen, 2015; Rexin et al., 2015). However, the specific downstream signaling targets and intersecting pathways with TOR kinase in plants are still not completely understood, especially as they relate to control of metabolism. Although the *Arabidopsis thaliana* TOR gene *AtTOR* is essential (Menand et al., 2002), conditional silencing resulted in early senescence with a decrease in photosynthesis linked to chlorophyll breakdown (Deprost et al., 2007) along with other metabolite changes reflecting altered carbon metabolism (Deprost et al., 2007; Ren et al., 2012; Caldana et al., 2013; Rexin et al., 2015). In Arabidopsis, regulation by sugars is upstream of TOR with glucose activating TOR and promoting cell proliferation in root meristems (Xiong et al., 2013). Overall, the roles of TOR in controlling carbon metabolism remain relatively unexplored in photosynthetic eukaryotes including algae where there is a growing interest in harnessing photosynthetic metabolism for increased biomass accumulation or as a feedstock for bioenergy (Hu et al., 2008; Merchant et al., 2012; Markou and Nerantzis 2013; Mayfield and Golden, 2015; Scranton et al., 2015).

In some species, including Chlamydomonas, TOR can be inhibited by the macrolide drug rapamycin, which has proven to be a pivotal tool for investigating TOR signaling (Crespo et al., 2005; Loewith and Hall, 2011; Rexin et al., 2015). Although Chlamydomonas is sensitive to rapamycin, at saturating drug concentrations cells grow slowly but do not arrest growth completely (Crespo et al., 2005). A screen for rapamycin resistance mutations identified alleles of *FKB1* that encode an ortholog of FK506 binding protein FKBP12 (Crespo et al., 2005; Vallon, 2005), a conserved peptidyl prolyl isomerase that forms a ternary complex with rapamycin and TORC1 and is required for rapamycin-mediated TOR inhibition (Heitman et al., 1991; Brown et al., 1994; Sabatini et al., 1994). Having a haploid genome and well developed molecular genetic tools, Chlamydomonas is a promising unicellular model organism in which to pursue functional studies of TOR kinase signaling and photosynthetic growth control.

Here, we used insertional mutagenesis in Chlamydomonas to screen for rapamycin-hypersensitive mutants. In doing so, we identified a loss-of-function mutation in *VIP1*, a gene encoding a conserved protein with predicted diphosphoinositol phosphate kinase activity whose function has not previously been linked to TOR signaling. Levels of $InsP_7$ and $InsP_8$, the predicted products of VIP1 kinase, were reduced in *vip1-1*, suggesting that these InsPs are required for cell growth in conjunction with TOR kinase activity. Unexpectedly, rapamycin hypersensitivity of *vip1-1* mutants required the presence of acetate in its growth media and the mutant cells were also found to have altered levels of tricarboxylic acid (TCA) cycle intermediates and increased levels of neutral lipids compared with wild-type cells. Our findings have implications for carbon partitioning and metabolic control by TOR and InsPs in other eukaryotes where these signaling systems are conserved and may provide a means of manipulating carbon flux and increasing yields of valuable storage compounds in algae and crop plants.

RESULTS

Isolation of Rapamycin-Hypersensitive Mutants from Chlamydomonas

A previous screen for rapamycin resistance yielded only *fkb1* mutants (Crespo et al., 2005), so we instead screened for rapamycin hypersensitivity among a population of insertional mutants (Galván et al., 2007) generated with the marker *aph7″* that confers resistance to the drug hygromycin (hygR phenotype) (Berthold et al., 2002). We anticipated that rapamycin hypersensitivity might result when growth-related processes that are regulated or coregulated by TOR are impaired. Our wild-type strains (CC-1690 and CC-1691) and most strains that we have tested show slowed but not completely inhibited growth in the presence of rapamycin, with saturation occurring at 500 nM to 1 μM (Crespo et al., 2005). We transformed and screened around 60,000 insertional mutants in CC-1690 for arrested or reduced growth in 500 nM rapamycin but normal growth in its absence (Figure 1A; see Methods). After retesting initial positives, we found only two mutants that had a consistent rapamycin hypersensitive (rapHS) phenotype, one of which, 266F3 (later found to be caused by insertion in the *VIP1* locus and designated *vip1-1*), is the focus of this study.

Among 600 total progeny from a backcross to a wild-type strain, we found consistent cosegregation of the rapHS phenotype with the hygR insertion (Figure 1B). We next tested whether the rapHS phenotype was dependent on the presence of the FKBP12 protein encoded by *FKB1*. *fkb1 vip1-1* double mutants were completely insensitive to rapamycin, indicating that the rapHS phenotype in *vip1-1* results from impaired TOR kinase signaling rather than off-target effects of rapamycin (Figure 1C). Further supporting the specificity of the mutant phenotype was our finding that *vip1-1* growth had a similar hypersensitivity to two other TOR kinase inhibitors with different inhibitory mechanisms from rapamycin, AZD8055 and Torin1 (Figure 1A) (Thoreen et al., 2009; Chresta et al., 2010).

We used adaptor-mediated PCR to identify a simple insertion of the HygR marker in the 11th coding exon of Cre03.g185500, whose predicted protein is related to a family of diphosphoinositol pentakisphosphate kinases also known as VIP proteins that will be described below (Figure 1D). The 266F3 mutation in Chlamydomonas was therefore designated *vip1-1*. Vegetative diploids with genotypes *VIP1/VIP1*, *vip1-1/VIP1*, and *vip1-1/vip1-1* were constructed and tested to reveal that the *vip1-1* mutation is a loss-of-function allele that is completely recessive to the wild-type allele (Supplemental Figure 1).

We cloned the ~11-kb wild-type *VIP1* genomic locus and used it to construct complementation vectors that contain a paromomycin resistance marker (ParoR) for selection (Sizova et al., 2001) and either unmodified *VIP1* (pVIP1) or a version of *VIP1* with an N-terminally encoded OLLAS peptide epitope tag (pOL-VIP) (Park et al., 2008) (Figure 1D; see Methods). Among >500 control transformants of *vip1-1* using an empty vector, we never observed complementation of the rapHS phenotype, whereas among transformants that received either pVIP1 or pOL-VIP1, we observed restoration of wild-type or near wild-type growth in the presence of rapamycin at a rate of ~3%, pVIP1 (2/80) and pOL-VIP1 (15/480) (Figure 1A). In transformants complemented with pOL-VIP1, we detected a single band

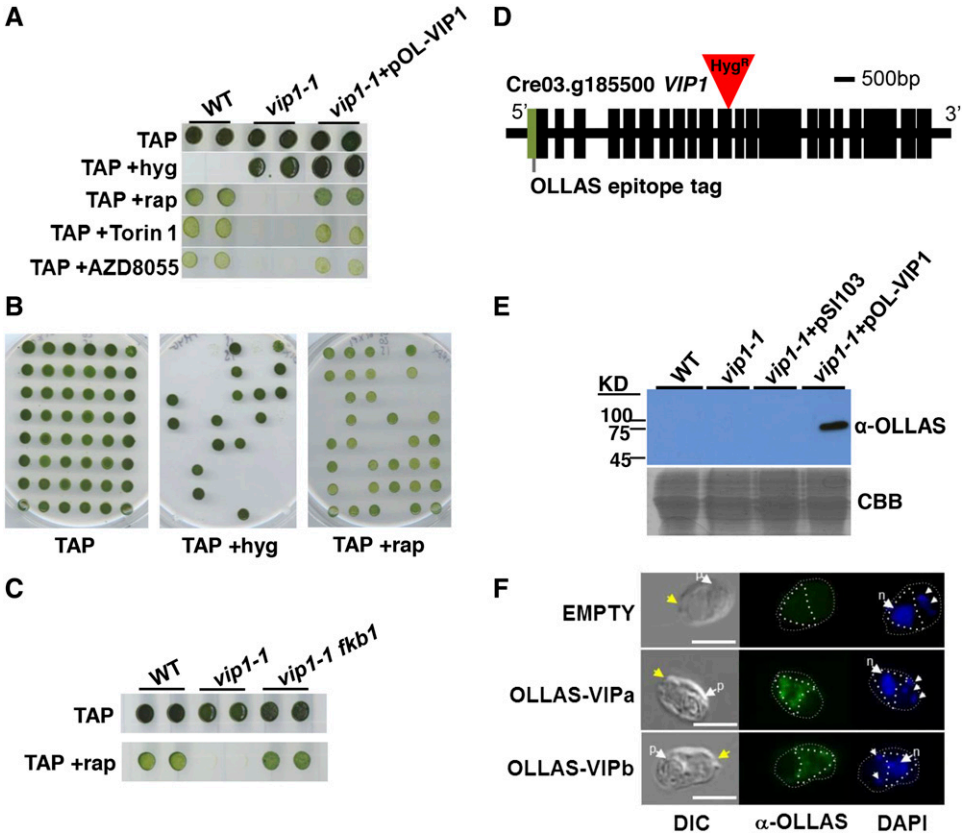

Figure 1. Identification of the Rapamycin-Hypersensitive Mutant *vip1-1*.

(A) Growth of the wild type, *vip1-1*, and *vip1-1* complemented with epitope-tagged construct pOL-VIP1 spotted onto TAP agar plates with hygromycin (+Hyg), 500 nM rapamycin (+rap), 500 nM Torin 1, or 500 nM AZD8055.

(B) Example of 48 random progeny from *vip1-1* backcrossed to a wild-type strain that were spotted onto TAP plates supplemented as in **(A)** and scored for hygromycin resistance and rapamycin sensitivity.

(C) The wild type, *vip1-1*, and *vip1-1fkb1* double mutants scored for rapamycin sensitivity as in **(A)** and **(B)**.

(D) Schematic representation of the CrVIP1 locus and *vip1-1* insertion. Tall rectangles represent exons. The inverted red triangle marks the pHyg insertion in the 11th exon. The light green shaded rectangle indicates the position of the OLLAS tag in pOL-VIP1.

(E) Upper panel is α-OLLAS immunoblot of the indicated strains shown in **(A)** plus *vip1-1* strain transformed with an empty vector control plasmid (pSI103). Migration of protein molecular weight markers is indicated on the left. Lower panel shows a SDS-PAGE gel loaded the same as in the upper panels and stained with Coomassie blue (CBB).

(F) Indirect immunofluorescence using OLLAS antibody (α-OLLAS) showing staining of an untagged control cell (top panel) and OLLAS-VIP expressing cells from two independently derived complemented strains. Left to right are DIC images, α-OLLAS signal in green, and 4′,6-diamidino-2-phenylindole (DAPI) signal in blue. Yellow arrows indicate apical ends of cells with flagella. White arrows labeled (p) are pyrenoids and (n) are nuclei. Small arrows mark chloroplast nucleoids. White dashed and dotted lines outline cell perimeter and cytoplasmic region stained by α-OLLAS antibody, respectively. Bars = 7.5 μm.

on immunoblots probed with anti-OLLAS antibodies migrating at the predicted size of tagged VIP1 (~170 kD) (Figure 1E). The same antibody was used in immunofluorescence experiments on fixed samples to localize VIP1 primarily to the cytoplasm (Figure 1F). We conclude that the rapHS phenotype of *vip1-1* is caused by a loss-of-function insertion mutation that either removes or impairs a cytosol-localized VIP1 protein.

VIP1 Encodes a Predicted Diphosphoinositol Pentakisphosphate Kinase

The predicted Chlamydomonas VIP1 protein (CrVIP1) showed high-scoring BLASTP similarity to a conserved family of eukaryotic diphosphoinositol pentakisphosphate kinases of the VIP family (Mulugu et al., 2007; Desai et al., 2014; Laha et al., 2015). VIP proteins contain two conserved domains, an ATP_GRASP domain (pfam 13535) that is predicted to have inositol diphosphate kinase activity (Mulugu et al., 2007; Fridy et al., 2007; Lin et al., 2009; Pöhlmann et al., 2014) followed by a histidine phosphatase domain (pfam 00328) that in CrVIP1 is interrupted with nonconserved sequences (Figure 2A). A more thorough search revealed a second but divergent VIP-related protein in Chlamydomonas that we designate CrVIP2. To better understand the phylogenetic relationships between CrVIP1, CrVIP2, and other eukaryotic VIP proteins, we constructed a phylogeny using the Chlamydomonas VIP putative paralogs and a diverse set

of VIP homologs from other taxa (Figure 2B). Overall, the phylogeny matches the scenario of at least one *VIP* gene being present at the base of the eukaryotic radiation and undergoing independent paralogous duplications in several lineages, including chlorophyte algae where the duplication was present in the ancestor of Chlamydomonas and its multicellular relative *Volvox carteri.* Additional independent duplications were found in the land plants with evidence for at least one event in monocots (*Oryza sativa*) and another in dicots (Arabidopsis) (Figure 2B; Supplemental Data Set 1).

With the exception of $InsP_6$ (phytic acid), which accumulates to high levels in many plant seeds, higher order InsPs ($InsP_4$, $InsP_5$, $InsP_7$, and $InsP_8$) are typically low abundance molecules with diverse roles in intracellular signaling (Raboy, 2003; Barker et al., 2009; Monserrate and York, 2010; Gillaspy, 2011; Wilson et al., 2013; Williams et al., 2015; Livermore et al., 2016). VIP1 is predicted to pyrophosphorylate $InsP_6$ at the 1,3 positions, generating 1PP-$InsP_5$ (In1sP_7) and possibly 1,3PP-$InsP_4$ (InsP8) (Figure 2C) (Lin et al., 2009). Besides VIP proteins, we identified homologs of other inositol polyphosphate (InsP) biosynthetic enzymes in Chlamydomonas that are predicted to carry out sequential conversion of $InsP_3$ to $InsP_4$, $InsP_5$, $InsP_6$, $InsP_7$, and $InsP_8$ (Figure 2C). We note that unlike fungi/animals/amoebae, which all contain two distinct families of enzymes capable of producing pyrophosphorylated inositols (IP6K/KCS1 and VIP), green algae and land plants appear to only contain the VIP family (Williams et al., 2015).

vip1-1 Mutants Have Defects in $InsP_7$ and $InsP_8$ Accumulation

The predicted products of CrVIP1, $InsP_7$ and $InsP_8$, are usually the lowest abundance InsPs in eukaryotic cells and difficult to detect (Bennett et al., 2006; Losito et al., 2009; Lin et al., 2009; Desai et al., 2014). Sensitive in vivo labeling procedures for InsP detection using radiolabeled 3H-inositol have been successful in other species (Azevedo and Saiardi, 2006; Stevenson-Paulik et al., 2006), but proved unfeasible in Chlamydomonas, which does not take up this precursor. Furthermore, InsPs were not abundant enough in Chlamydomonas lysates to enable utilization of electrophoretic separation and staining detection methods that do not require labeling (Losito et al., 2009). Therefore, we developed a reproducible and sensitive liquid chromatography and tandem mass spectrometry (LC-MS/MS) method for detection and discrimination of different InsP species calibrated using commercial standards and a synthetic InsP (3-deoxy-3-fluoro-D-myo-inositol 1,4,5 trisphosphate [3-fluoro-$InsP_3$]), as an internal standard for normalization (see Methods). Applying this method to InsPs purified from whole-cell lysates of Chlamydomonas, we compared profiles of wild-type, *vip1-1*, and complemented *vip1-1*+pOL-VIP1 strains.

Using LC-MS/MS, we were able to reproducibly detect six major InsP species in wild-type extracts: $InsP_3$, $InsP_4$, $InsP_5$, $InsP_6$, $InsP_7$, and $InsP_8$. Although we currently cannot discriminate between InsP stereoisomers using our method, the conserved repertoire of predicted InsP biosynthetic enzymes in Chlamydomonas (Figure 2C) suggests that the same spectrum of InsPs will be produced in Chlamydomonas as in plants. According to our analysis, we found $InsP_6$ to be the most abundant species while $InsP_7$ and $InsP_8$ were the least abundant (Figure 3A). Moreover, *vip1-1* cells had significant defects in accumulation of $InsP_7$ and $InsP_8$ that were present at 20 to 30% of wild-type levels and fully or partially restored in complemented strains (Figure 3A, insets). The most abundant InsP species in Chlamydomonas, $InsP_6$, was somewhat reduced in *vip1-1*, while levels of three lower order InsPs ($InsP_3$, $InsP_4$, and $InsP_5$) were not significantly altered (Figure 3A). We hypothesize that residual $InsP_7$ and $InsP_8$ detected in *vip1-1* is due to the activity of CrVIP2 (Figures 2B and 2C) whose mRNA is expressed at <10% of the level of *CrVIP1* mRNA under diurnal growth conditions (Zones et al., 2015). Together, our data support the predicted role of Chlamydomonas VIP1 as a diphosphoinositol kinase whose function in $InsP_7$ and $InsP_8$ biosynthesis is acutely required for cell growth when the TOR signaling pathway is impaired.

Impaired TOR Signaling Alters InsP Levels

Our results showed a functional interaction between TOR kinase signaling and InsPs; however, they did not indicate whether one signaling pathway is dependent on the other or if they both converge on a common target(s). While tools for direct measurement of TOR kinase activity (i.e., confirmed phosphorylation substrates) are not currently available for Chlamydomonas, we could measure the impact of impaired TOR signaling on intracellular InsP levels. We grew wild-type and *vip1-1* cultures under mixotrophic conditions (TAP) and measured InsPs after rapamycin addition for 1 and 12 h. One hour is the earliest time point when growth is measurably reduced by rapamycin, and by 12 h, wild-type cells have begun to acclimate to rapamycin, while *vip1-1* mutants are still growth arrested (Figure 3B). For wild-type cells, the response of InsPs to rapamycin involved a transient drop in $InsP_5$, $InsP_6$, $InsP_7$, and $InsP_8$ at 1 h, with partial recovery after 12 h (Figure 3B). On the other hand, $InsP_3$, and to some extent $InsP_4$, became elevated over basal levels in the wild type after 12 h in rapamycin (Figure 3B). For rapamycin-treated *vip1-1*, we saw no change in $InsP_3$, but major reductions in other InsP species, including $InsP_6$ that was reduced by more than 10-fold and a near complete absence of residual $InsP_7$ and $InsP_8$ (Figure 3B). Taken together, our results show that impaired TOR signaling leads to changes in InsP levels and suggests that InsPs are downstream of TOR signaling. Moreover, when TOR signaling is impaired in *vip1-1* cells, $InsP_7$ and $InsP_8$ become nearly undetectable and growth arrests completely, suggesting that these InsPs may play an essential role in cell growth. Additional studies will be required to test whether InsPs also act upstream of TOR kinase to influence its activity.

Interaction between *vip1-1* and TOR Signaling Is Carbon Source Dependent

When supplemented with acetate, Chlamydomonas cells generally grow faster while simultaneously downregulating rates of photosynthesis (Heifetz et al., 2000; Chapman et al., 2015). Growth of *vip1-1*, wild-type, and complemented strains on agar plates or in liquid media with and without acetate and rapamycin were compared (Figure 4). While *vip1-1* grew at similar rates as

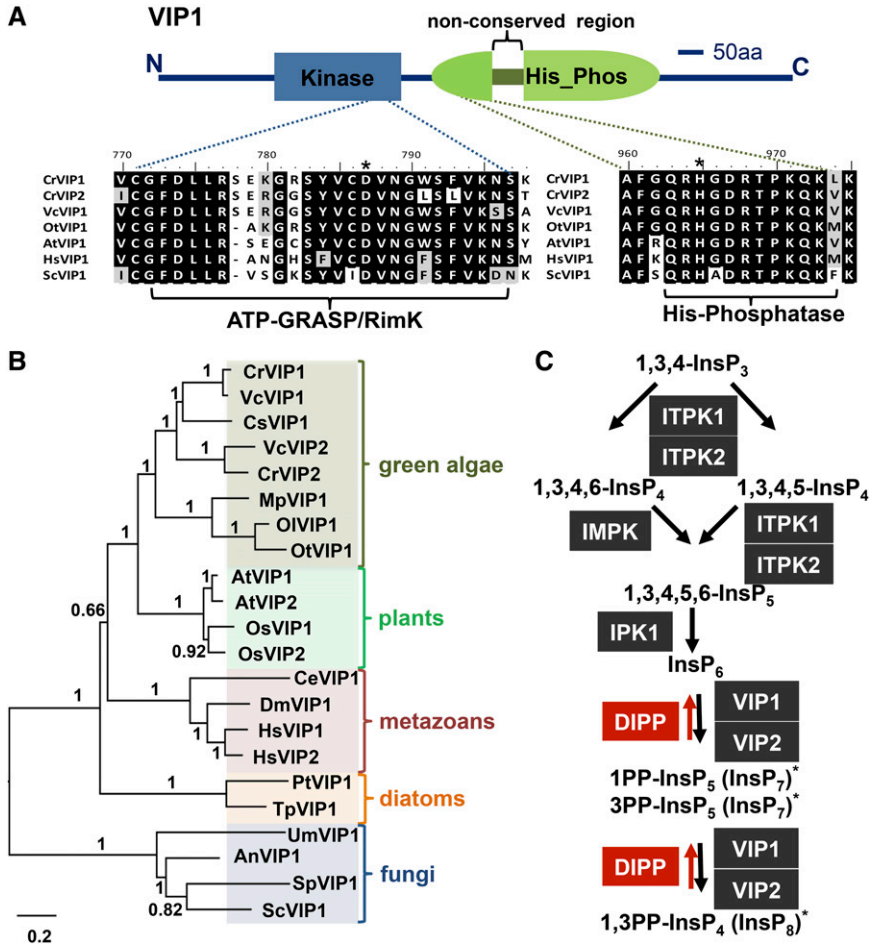

Figure 2. Domain Structure, Phylogenetic Analysis of VIP1, and Predicted InsP Pathway in Chlamydomonas.

(A) Schematic representation CrVIP1 domain structure from N terminus (N) to C terminus (C) with kinase and histidine phosphatase domains labeled. Below the schematic are alignments of predicted catalytic regions of VIP family members from *Chlamydomonas reinhardtii* (CrVIP1 and CrVIP2), *Volvox carteri* (VcVIP1), *Ostreococcus tauri* (OtVIP1), *Arabidopsis thaliana* (AtVIP1), *Homo sapiens* (HsVIP1), and *Saccharomyces cerevisiae* (ScVIP1). Asterisks indicate predicted catalytic residues. aa, amino acids.

(B) Neighbor-joining phylogeny of VIP proteins from representatives of different eukaryotic taxa. Bootstrap values for each node from 1000 replicates are indicated as decimal fractions. Scale bar units are substitutions per site. The alignment used to generate the phylogeny is presented in Supplemental Data Set 1.

(C) Sequential phosphorylation of 1,3,4 $InsP_3$ is depicted with black shaded boxes representing predicted InsP kinases, black arrows representing phosphorylation reactions, red shaded boxes representing predicted InsP phosphatases, and red arrows representing dephosphorylation reactions. Asterisks represent predicted stereoisomers formed by VIP1 or VIP2 (see main text for details).

wild-type or complemented strains under both phototrophic (TP media) and mixotrophic (TAP media) conditions without rapamycin (Figures 4A, 4B, and 4D), its response to rapamycin was acetate dependent (Figures 4A, 4C, and 4E). In media with acetate and rapamycin, growth of *vip1-1* was completely arrested (Figures 4A and 4E) and cell viability was reduced by around 20 to 30% (Figures 4F and 4G), while wild-type and complemented strains showed only transiently slowed growth (Figure 4E) and also had a 20 to 30% reduction in viability (Figures 4F and 4G). However, in media without acetate, *vip1-1* responded to rapamycin similarly to wild-type and to complemented strains with slowed but not arrested growth (Figures 4A to 4C). Overall, our data suggest that defects associated with acetate metabolism may underlie the *vip1-1* phenotype of hypersensitivity to TOR inhibition.

vip1-1 Partially Uncouples Neutral Lipid Accumulation from Nitrogen Starvation and Acetate Assimilation

The effect of acetate on *vip1-1* prompted us to assess whether the two major storage carbon pools in Chlamydomonas, neutral lipids and starch, were altered in the mutant. For typical wild-type strains, Nile Red stained lipid bodies are most readily detectable in acetate-containing media when cells have been starved for

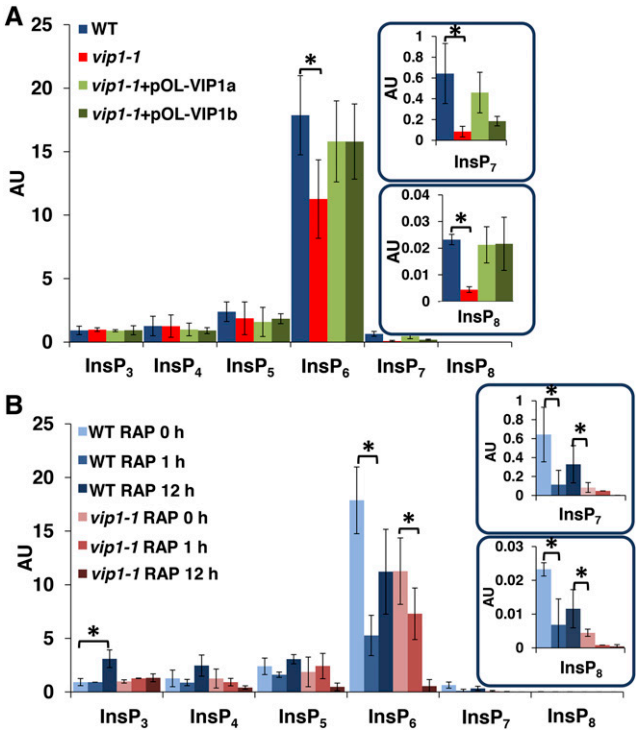

Figure 3. *vip1-1* Is Defective in the Production of $InsP_7$ and $InsP_8$.

Bar graphs scaled in arbitrary units (AU) and normalized with a standard, 3-fluoro-InsP3, showing relative levels of InsP species extracted from indicated strains and measured using mass spectrometry.

(A) Data are from the wild type, *vip1-1*, and two complemented strains, *vip1-1+pOL-VIP1a* and *vip1-1+pOL-VIP1b*, growing exponentially in TAP. Insets for $InsP_7$ and $InsP_8$ have magnified *y* axis scales.

(B) Comparison of InsP profiles in wild-type and *vip1-1* cultures growing in TAP (0 h) or TAP treated with 500 nM rapamycin for 1 or 12 h. Error bars indicate SD from at least three biological replicates. Asterisks represent significant differences ($P < 0.05$) evaluated using Student's *t* test.

nitrogen (TAP -N) (Figure 5A). By contrast, in *vip1-1* strains, we always observed lipid bodies, even under conditions where few or no lipid bodies were detectable in wild-type cells, such as in actively growing cultures with nitrogen-replete media (TP and TAP) (Figure 5A). Quantitative measurements of total lipids showed increased levels in *vip1-1* strains compared with the wild type under the same growth conditions as described above with significant restoration of wild-type levels in complemented strains (Figures 5B and 5C). Starch levels of *vip1-1* were not significantly different from wild-type strains growing in TAP, where lipid overaccumulation was detectable (Figure 5D).

The Nile Red staining results suggested that some or all of the excess lipids in *vip1-1* were triacylglycerol (TAG), the major neutral storage lipid form in Chlamydomonas (Wang et al., 2009; Siaut et al., 2011; Merchant et al., 2012; Goodenough et al., 2014). To compare TAG levels in *vip1-1* and the wild type, we used thin-layer chromatography (TLC) separation and iodine staining of separated total lipids (Figure 6A) or quantitative gas chromatography on transesterified purified TAGs from cells grown under three conditions: TAP (exponential phase), TAP with rapamycin (12 h), and TAP under nitrogen starvation (TAP -N; 12 h) (Figure 6B). In each case, we found increased TAG content in *vip1-1* compared with the wild type, suggesting that the mutant is either additive with TAG-inducing stimuli or accelerates the response to such stimuli. While the relative distributions of acyl chain species of total lipids from TAP-grown wild type and *vip1-1* were not detectably different from each other, the fractional composition of acyl chain species in the purified TAG fraction from *vip1-1* was different from the wild type: *vip1-1* TAGs were de-enriched for C16:0 and enriched for C16:4, C18:1, C18:2, and C18:3 (Figure 6C). C16:4 acyl chains have been reported to be almost exclusively found in the chloroplast of Chlamydomonas (Giroud et al., 1988), suggesting a direct or indirect connection to altered plastid lipid metabolism in *vip1-1*. Consistent with the possibility of altered chloroplast lipid content or lipid metabolism, we found in *vip1-1* an ~20% decrease in total galactolipids, a type that are found only in chloroplast membranes of Chlamydomonas. By contrast, we measured no significant changes in phospholipids that are found in plasma membranes and endomembranes (Giroud et al., 1988) (Figures 6D and 6E). In summary, our data show that storage lipids are increased in *vip1-1* and that their accumulation is partially decoupled from inducing signals such as N starvation or stress that are required to trigger TAG accumulation in wild-type cells.

Altered TCA Metabolism in *vip1-1* and Modulation of InsPs by Carbon Source

The altered lipid accumulation phenotypes of *vip1-1* suggest that the mutant may also have underlying changes in carbon metabolism. Altered metabolite levels can point to altered flux in a corresponding pathway, though they do not provide direct information on rate changes. We focused on the TCA cycle as it is the part of central carbon metabolism most proximal to lipid biosynthesis and to acetate utilization (Figure 7). We grew the wild type and *vip1-1* with and without acetate (TAP and TP media) and compared TCA metabolite levels between strains and growth conditions. Focusing on mixotrophic conditions (TAP), we found significant reductions of citrate, aconitate, malate, and acetyl-coA in *vip1-1* (Figure 7, dark-blue and dark-red bars). *vip1-1* cells also responded differently from the wild type to phototrophic conditions where we found 2-fold or greater increases in aconitate, succinate, and fumarate (Figure 7, light-blue and pink bars). As expected, wild-type cells responded to acetate with alterations in levels of TCA cycle intermediates (Heifetz et al., 2000; Boyle and Morgan, 2009; Chapman et al., 2015), but *vip1-1* does not undergo the same responses, indicating potential alterations in TCA flux in this mutant that may be tied to altered lipid metabolism and its other phenotypes.

Modulation of Intracellular InsPs in Response to Growth Conditions and TOR Signaling

The predicted products of VIP1, $InsP_7$, and $InsP_8$ are potential signaling molecules whose levels are perturbed in *vip1-1* strains. Moreover, this perturbation impacts central carbon metabolism and lipid accumulation and appears to do so acutely when TOR kinase signaling is also inhibited. These observations suggest that InsPs may be used in Chlamydomonas as signals for responding

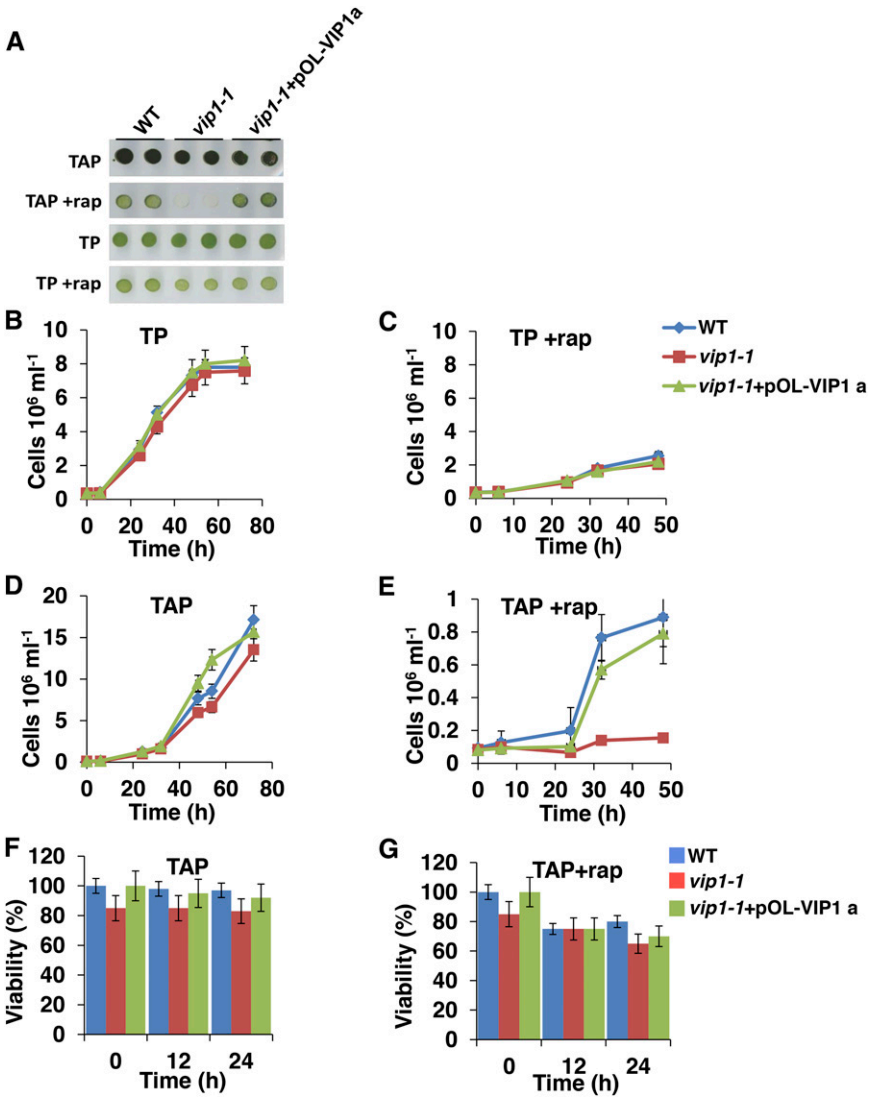

Figure 4. Carbon Source-Dependent Growth Inhibition of *vip1-1* by Rapamycin.

(A) Growth of the indicated strains (see Fig. 1A) spotted onto agar plates with and without acetate (TAP and TP, respectively) in the absence or presence of 500 nM rapamycin (+rap).

(B) to **(E)** Growth curves from liquid cultures of strains in **(A)**.

(F) and **(G)** Viability of the wild type, *vip1-1*, and *vip1-1*+pOL-VIP1 in the presence and absence of rapamycin. Colony-forming units (CFUs) were measured at 0, 12, and 24 h and used to calculate viability (CFUs/number of cells plated). Error bars indicate SD from two biological replicates and three technical replicates.

to and/or controlling carbon metabolism. If so, the InsP profiles, including the products of VIP1 ($InsP_7$ and $InsP_8$), would be expected to change according to growth conditions such as presence/absence of acetate. Indeed, we found that in wild-type cells there were significant changes in InsPs in response to acetate. Wild-type $InsP_3$ levels were 10-fold lower in TAP versus TP, while levels of $InsP_6$, $InsP_7$, and $InsP_8$ behaved in an opposite manner with moderately higher levels in TAP (Figure 8A). Thus, InsP profiles of wild-type cells, including the predicted VIP1 kinase substrate ($InsP_6$) and VIP1 kinase products ($InsP_7$, $InsP_8$), were modulated by the presence and absence of external acetate. *vip1-1* cells also responded to the presence and absence of acetate but had significant differences from wild-type cells. In the case of $InsP_3$, *vip1-1* cells had near wild-type levels in acetate-containing media but did not show the same degree of elevation in media without acetate (Figure 8A). As expected, the levels of $InsP_7$ and $InsP_8$ in *vip1-1* were severely decreased under all conditions compared with the wild type. On the other hand, the levels of $InsP_6$ were much lower in *vip1-1* cells grown in TP versus TAP, while in wild-type cells $InsP_6$ levels changed only modestly between media with and without acetate. In summary, InsPs in Chlamydomonas, including predicted VIP1 kinase substrates and products, showed

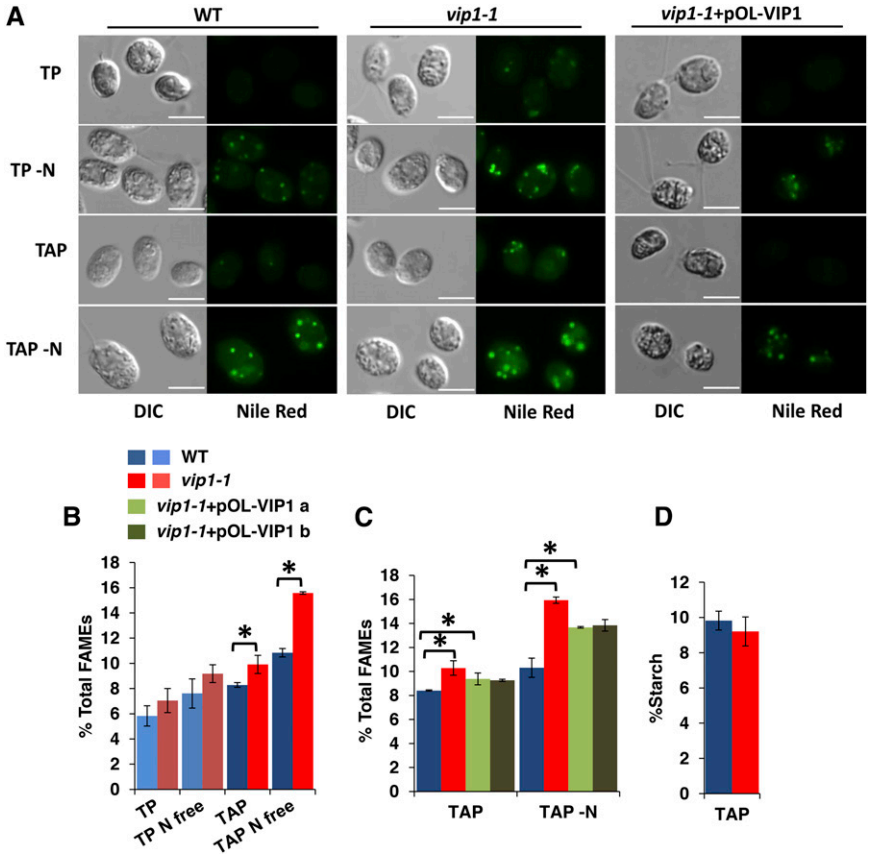

Figure 5. Lipid Overaccumulation in *vip1-1*.

(A) Lipid bodies of strains growing in indicated media were stained with Nile Red and imaged using DIC and wide-field fluorescence microscopy with a standard GFP/FITC filter set. All images were taken using identical microscope settings. Bars = 7.5 μm.
(B) GC-FID quantitation of total FAMEs from the wild type and *vip1-1* under conditions used in **(A)**. All values are normalized to dry cell weight. Error bars indicate SD from three biological replicates. Asterisks represent significant differences ($P < 0.05$) between means evaluated using Student's *t* test.
(C) GC-FID quantitation of total lipids in the wild type, *vip1-1*, and two complemented strains (*vip1-1*+pOL-VIP1 a and b) in TAP and TAP -N labeled as in **(B)**.
(D) Graph of starch content of wild-type and *vip1-1* strains grown in TAP and normalized by dry cell weight. Error bars indicate SD from five replicates.

complex acetate-dependent changes in accumulation profiles in a manner that is consistent with InsPs acting as signals for growth metabolism and acetate utilization. Moreover, the same set of InsPs whose levels changed most in response to carbon source in wild-type cells, including $InsP_7$ and $InsP_8$, were the most affected by the *vip1-1* mutation. Together, our results support a role for InsPs as intracellular signals governing carbon metabolism in Chlamydomonas (Figure 8B).

DISCUSSION

Chlamydomonas VIP1 Provides an Entrée into Inositol Polyphosphate Signaling in Green Algae

Higher order InsPs and the kinases that synthesize them are largely conserved across eukaryotes (Irvine and Schell, 2001; Raboy, 2003; Williams et al., 2015). In fungi, the roles of InsPs have been dissected using mutants that block different steps in the biosynthetic pathway. $InsP_7$ and $InsP_8$ are produced by VIP1 and/or KCS1 kinases whose animal homologs are PP-InsP5K and InsP6K, respectively, and play diverse roles in cell physiology, including signaling phosphate starvation, telomere length control, DNA repair, autophagy, environmental stress responses, cytoskeletal dynamics, and ribosome biogenesis (Bennett et al., 2006; Shears, 2009; Tsui and York, 2010; Wundenberg and Mayr, 2012; Wilson et al., 2013; Thota and Bhandari, 2015; Livermore et al., 2016).

In plants, InsPs are of special interest because $InsP_6$ (phytic acid) is agronomically important as a high-abundance phosphate storage compound in seeds (Raboy, 2003), and other InsPs have recently been investigated for potential roles in hormone signaling and plant defense (Tan et al., 2007; Mosblech et al., 2008, 2011; Sheard et al., 2010; Laha et al., 2015). Green algae and land plants encode enzymes required to successively convert $InsP_3$ to $InsP_7$ and $InsP_8$ (Figure 2B) (Loewus and Murthy, 2000; Raboy, 2003; Gillaspy, 2013; Williams et al., 2015), though they are missing the KCS1/InsP6K family that pyrophosphorylates $InsP_6$ or $InsP_7$ on

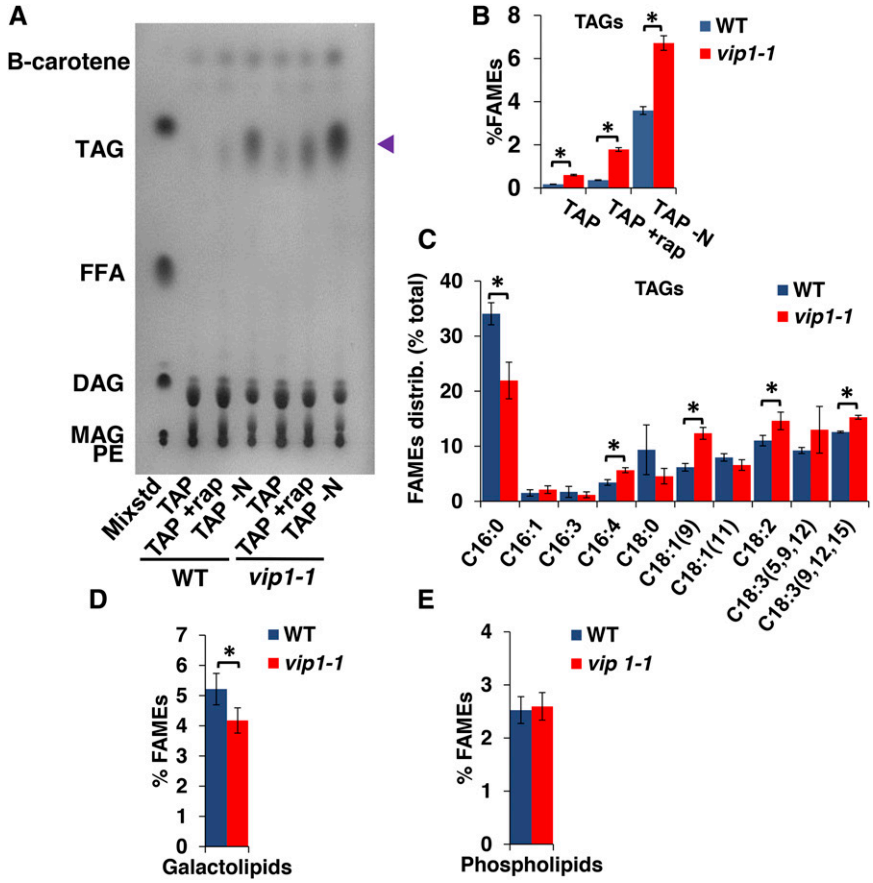

Figure 6. Increased TAG and Decreased Galactolipids in *vip1-1*.

(A) TLC separation and iodine staining of different lipid classes from total lipids of wild-type and *vip1-1* cells growing in TAP, TAP supplemented with rapamycin for 12 h (+rap), or transferred to TAP-N for 12 h. The left-most lane contains a mixture of standards (Mixstd) whose constituents are abbreviated as follows: PE, phosphatidyl ethanolamine; MAG, monoacylglycerol; DAG, diacylglycerol; FFA, free fatty acids; TAG, triacylglycerol. The identification of β-carotene in the fastest migrating position was done separately using a purified standard. Blue arrowhead on right indicates migration of TAGs.
(B) Quantitation of FAMES derived from purified TAGs and normalized by dry cell weight for strains shown in **(A)**. Errors bars indicate SD from five replicates.
(C) Relative distribution (percent total) of acyl group types from TAG fraction of wild-type and *vip1-1* strains.
(C) and **(D)** Percentage of FAMEs in galactolipid and phospholipid fractions purified from the wild type and *vip1-1* and normalized by dry cell weight. Error bars indicate SD from at least three biological replicates. Asterisks represent significant differences ($P < 0.05$) between means evaluated using Student's *t* test.

position 5 of the inositol ring, an activity which is distinct from the activity of VIP proteins that act on the 1/3 positions (Lin et al., 2009) (Figure 2C). The two VIP paralogs of Arabidopsis (AtVIP1 and AtVIP2; also called AtVIH1 and AtVIH2) can complement a yeast *vip1* deletion (Desai et al., 2014) and are required for jasmonate defense signaling (Laha et al., 2015). A QTL for vitamin E levels also mapped to one of the two Arabidopsis VIP genes (At3g01310) (Gilliland et al., 2006), though a connection between InsPs and vitamin E has not been directly established. Other metabolic phenotypes in plants defective for VIP genes have not been reported; however, interaction between $InsP_7$ and SPX domain proteins including regulators of phosphate homeostasis have been recently found (Wild et al., 2016). We note that the media used in our study contain excess inorganic phosphate making phosphate metabolism unlikely to underlie the growth and metabolic defects we observed in *vip1-1*.

InsPs in green algae were previously examined in two species of Chlamydomonas, *C. reinhardtii* and *C. eugametos* (also called *C. moewusii*), that are quite distantly related (Pröschold et al., 2001). In both species, $InsP_3$ appears to play a conserved role as a second messenger and effector of cytosolic calcium influx that triggers deflagellation (Yueh and Crain, 1993; Quarmby and Hartzell, 1994; Munnik et al., 1998) and is also linked to light-dependent expression of *GSA*, a gene of the heme/chlorophyll biosynthetic pathway (Im and Beale, 2000). InsP kinase activities that can produce $InsP_4$, $InsP_5$, and $InsP_6$ have been found in extracts from *C. eugametos* (Irvine et al., 1992), but no roles for these higher order InsPs or evidence of pyrophosphorylated InsPs have been previously reported in green algae. Our identification of a mutation in the *C. reinhardtii VIP1* gene that causes defects in $InsP_7$ and $InsP_8$ accumulation provides a tool for dissecting the roles of VIP proteins and pyrophosphorylated InsPs in green algae with possible relevance for other eukaryotic

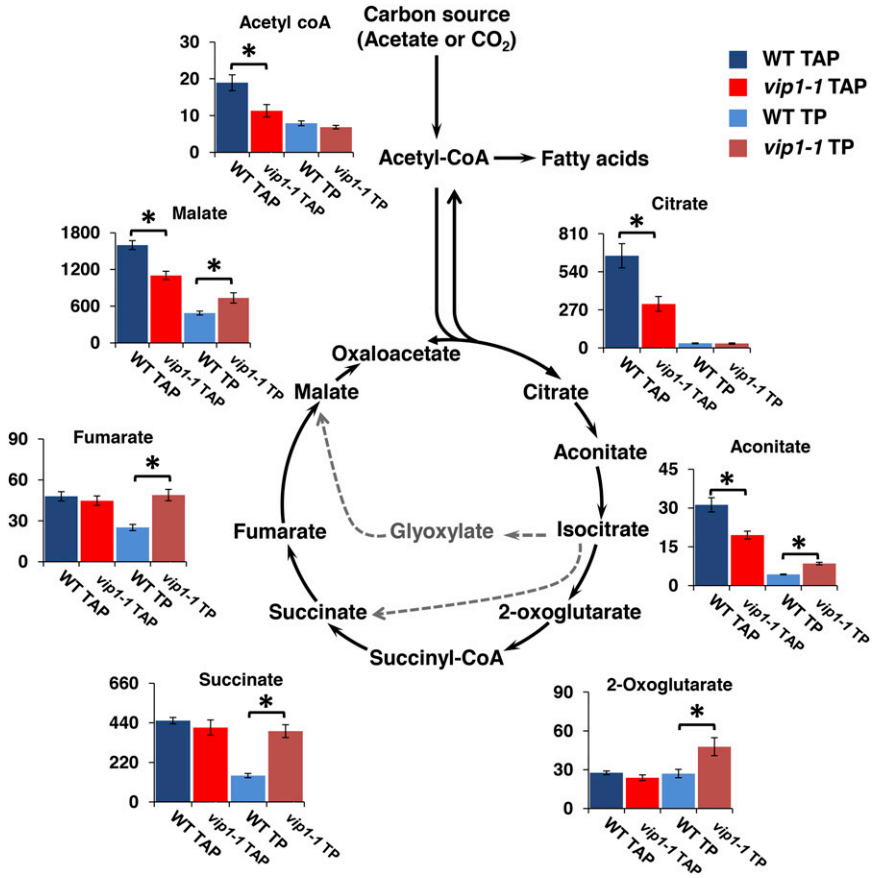

Figure 7. Altered Profiles of TCA Cycle Metabolites in *vip1-1*.

Diagram of TCA cycle with bar graphs showing levels of metabolites that were measured in the wild type and *vip1-1* growing mixotrophically in TAP or phototrophically in TP. Solid black arrows show the canonical respiratory TCA cycle where carbon is lost as CO_2; gray dashed arrows show the glyoxylate cycle where carbon is conserved for anabolic metabolism. *y* axes are measured in nmol/gFW. Error bars indicate SD from at least three biological replicates. Asterisks represent significant differences ($P < 0.05$) between means evaluated using Student's *t* test.

species, including plants that also contain VIP proteins but no KCS1/InsP6K-like proteins (Bennett et al., 2006; Desai et al., 2014; Williams et al., 2015). Despite *vip1-1* being a loss-of-function allele, the mutants still have some detectable $InsP_7$ and $InsP_8$ (Figures 3 and 8), indicating that there may be another route for $InsP_7$ and $InsP_8$ synthesis in these cells. A second predicted *VIP* gene, *VIP2* (Figures 2B and 2C), is the best candidate for producing residual $InsP_7$ and $InsP_8$ in *vip1-1.*

InsPs as a Metabolic Signal for Carbon Metabolism

Much attention has already been focused on the metabolic pathways of Chlamydomonas that are responsible for accumulation of TAGs as these are important end products for biofuel and biotechnology applications (Hu et al., 2008; Merchant et al., 2012; Liu and Benning, 2013; Goodenough et al., 2014). Previous studies have assessed the responses of metabolic genes and proteins under non-steady state conditions when TAG accumulates (Miller et al., 2010; Boyle et al., 2012; Msanne et al., 2012; Blaby et al., 2013; Wase et al., 2014) or identified mutants that are defective for TAG accumulation or catabolism (Li et al., 2012; Boyle et al., 2012; Tsai et al., 2014; Xie et al., 2014; Ngan et al., 2015; Kajikawa et al., 2015). The relationship between starch synthesis and TAGs has also been investigated, and it appears that fixed carbon can be shunted toward TAGs when starch synthesis is blocked (Li et al., 2010a, 2010b; Work et al., 2010; Siaut et al., 2011; Goodenough et al., 2014). One recently identified regulatory mutant, *tar1*, is defective in accumulation of lipid bodies in response to nutrient starvation, and the *TAR1* locus was shown to encode a YAK subtype DYRK family protein kinase (Kajikawa et al., 2015). The transcription factors PSR1 and NRR1 have also been postulated as regulators for lipid accumulation during nitrogen starvation (Boyle et al., 2012; Ngan et al., 2015), and the transcription factor CHT7 is required for TAG remobilization when starved cells are returned to nutrient-replete media (Tsai et al., 2014). To date, no putative regulatory mutants have been identified that uncouple TAG accumulation from nitrogen starvation or acetate supplementation as we observed in *vip1-1*, nor have regulatory mutants been described that cause increased TAG and lipid overaccumulation compared with wild-type cells.

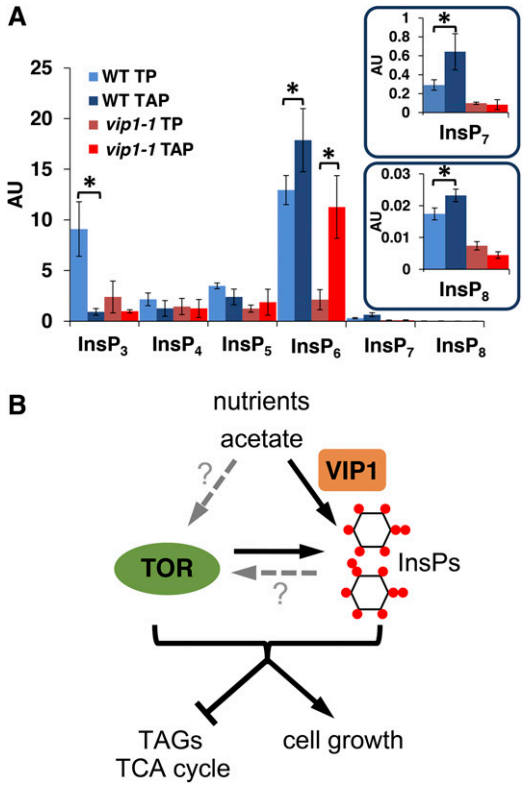

Figure 8. TOR and InsP Interact to Control Cell Growth, Acetate Metabolism, and Neutral Lipid Accumulation.

(A) Modulation of intracellular InsP levels by carbon source. Graphs labeled as in Fig. 3 showing InsP levels from the wild type and *vip1-1* growing in the presence or absence of acetate (TAP and TP, respectively).

(B) Summary figure of proposed relationships between carbon source (acetate), TOR, and InsPs produced by VIP1. Black arrows indicate interactions shown in this work (TOR signaling and carbon source influence InsP levels), while dashed gray arrows with question marks are possibilities that were not directly tested. TOR and the InsPs produced by VIP1 synergistically inhibit TAG accumulation (repression bar) and promote cell growth (arrow).

Under mixotrophic conditions (light+acetate), *vip1-1* cells completely arrested growth in the presence of rapamycin, while in phototrophic conditions (light only), rapamycin hypersensitivity was relieved (Figure 4), indicating an interaction between InsPs, TOR signaling, and carbon metabolism. Even in the absence of rapamycin, *vip1-1* mutants showed metabolic defects including overaccumulation of TAGs that were partially uncoupled from starvation or stress cues (Figures 5 and 6). We propose that InsPs, including those produced by VIP1 kinase, are used in Chlamydomonas as metabolic signals that interact with the TOR kinase signaling pathway to control growth and lipid storage in response to the availability of organic carbon (Figure 8B). Supporting this idea was our finding that the relative abundances of InsPs, including the predicted VIP1 products $InsP_7$ and $InsP_8$, changed significantly in wild-type cells growing under phototrophic versus mixotrophic conditions (Figure 8A) and their levels also responded to TOR inhibition by rapamycin (Figure 3B). The natural diversity of InsPs structural isomers (Irvine and Schell, 2001; Saiardi, 2012) and their rapid turnover could make them highly responsive signals for metabolic control.

Although *vip1-1* mutants do not appear to suffer from any acute metabolic tradeoffs, there are likely to be fitness defects in this mutant that emerge under specific conditions that have not been tested here. Importantly, the metabolic alterations in *vip1-1* that lead to increased TAG levels appear to be synergistic with other conditions that cause increased TAG accumulation such as nitrogen starvation or rapamycin treatment (Figures 6A and 6B). It remains to be determined whether the normal responses to stress and starvation are accelerated in *vip1-1* or if the mutant activates a parallel pathway for storage lipid accumulation. Two recent studies implicated the TCA pathway in carbon utilization and lipid accumulation. A Chlamydomonas mutant missing isocitrate lyase, a key enzyme in the glyoxylate shunt within the TCA cycle, was found to have acetate-specific growth defects and to overaccumulate lipids (Plancke et al., 2014). A metabolic modeling study also found that changes in TCA flux were required to maintain metabolic balance when switching from phototrophic to mixotrophic growth (Chapman et al., 2015). Our metabolite profiling results (Figure 7) further suggest that accumulation of lipids in *vip1-1* may be coupled to altered flux through the TCA cycle.

A Connection between Inositol Polyphosphates and the TOR Signaling Pathway in Chlamydomonas Is Revealed by *vip1-1*

Interactions between TOR signaling and InsP in yeast and animals have been suggested by several studies (Chakraborty et al., 2010; Kim and Guan, 2011) including roles for InsP kinases upstream (Nagata et al., 2005) and downstream of TOR (Worley et al., 2013). These findings are not mutually exclusive, but they do highlight the potential complexity of intracellular signaling pathways where feedback loops can connect signaling systems at different levels. To date there has been no connection made between TOR signaling in photosynthetic eukaryotes and InsPs. Interestingly, we found that rapamycin inhibition, even in wild-type cells, caused changes in InsP levels, meaning that at least part of the rapamycin hypersensitivity we see in *vip1-1* could be caused by defects in InsPs that act as effectors of TOR signaling (Figures 3B and 8B). The apparently complete elimination of detectable $InsP_7$ and $InsP_8$ in rapamycin-treated *vip1-1* cells is suggestive of an essential role for these InsPs in cell growth. We attempted to assess the effect of *vip1-1* on TOR kinase signaling using a commercial antibody that detects S6K (ribosomal protein S6 kinase) phosphorylation by TOR on a conserved site (Thr-389 in human S6K and Thr-932 in Chlamydomonas) and that has been used successfully in Arabidopsis (Xiong et al., 2013) but were unable to detect a specifically recognized cross-reacting protein in Chlamydomonas extracts. Nonconservation with the human S6K phospho-epitope at the −3 and −5 positions with respect to T389 may be partly responsible for this lack of cross-reactivity. Until TOR kinase activity assays are developed for Chlamydomonas, we cannot test the possibility that InsPs are also upstream of TOR signaling and/or function in a parallel pathway (Figure 8B). While the relationships between TOR and InsPs remain to be fully elucidated, the synergism between the two signaling systems that we uncovered may have relevance in other eukaryotes where both are conserved.

METHODS

Chlamydomonas reinhardtii Strains, Culture Conditions, and Viability Test

Strain CC-1690 wild-type *MT+* (Sager 21gr) (Sager, 1955) was used as parental strain to generate *vip1-1*. CC-1691 (Sager 6145c) wild-type *MT−* was used for segregation/linkage analysis and diploid generation described below. An *fkb1* mutant (originally named *rap2*) contains a disruption in the Cre13.g586300 locus and was kindly provided by Jose-Luis Crespo (Crespo et al., 2005). All cultures were maintained on TAP (Tris acetate phosphate) agar plates (Harris, 2009b). TP was prepared as TAP but omitting acetic acid and replacing Tris-base with Tris-HCl, pH 7.4. N-free media was prepared by omitting NH_4Cl. Liquid cultures were grown in 500-mL flasks at 25°C in temperature controlled water baths illuminated continuously from below with ~150 $\mu E\, m^{-2}\, s^{-1}$ LED lights (1:1 fluence ratio red [625 nm] and blue [465 nm]) and bubbled with air or air enriched with 0.5% CO_2 (v/v). Except where mentioned, experiments were done using cultures in exponential phase (1 to 2×10^6 cells/mL) that were maintained in exponential phase through frequent dilution (at least once per day). N-starved cultures were prepared by centrifuging and washing cells twice in the N-free media (TAP-N or TP-N) and then resuspending them in N-free media. Cultures were monitored for cell size and cell concentration using a Multisizer 3 Coulter Counter (Beckman).

Viability experiments were performed using cultures pregrown to mid-late exponential phase (2 to 8×10^6 cells/mL) and then diluted into the same media with or without rapamycin to a density of ~2×10^5 cells/mL. Rapamycin (LC Laboratories) was added to a final concentration of 500 nM from a 50 mM stock in DMSO. Viability for each sample was calculated by dividing the number of colony-forming units determined by plating on agar plates by the cell density measured in a Coulter Counter.

Mutant Screening

Insertional mutagenesis (Galván et al., 2007) with a hygromycin resistance gene, *aph7″* (Berthold et al., 2002), was used to generate mutants using wild-type parental strain CC-1690. Transformation was performed using electroporation modified from a published method (Shimogawara et al., 1998), as follows: 300 mL cultures in TAP were grown to a density of ~1×10^6/mL. Cells were harvested by centrifugation (4000 rcf, 5 min, room temperature) and resuspended at 3.5×10^8 /mL in TAP with 50 mM sorbitol. Next, 1 μg DNA and 300 μL of the cell suspension were placed into 4-mm cuvettes (Bio-Rad) prechilled on ice for 15 min, and then electroporated using a GenePulser Xcell (Bio-Rad), with settings of 800 V, 25 μF, and no resistance. Transformants were recovered in 10 mL TAP+50 mM sorbitol in low light for 16 h and then concentrated and spread on two TAP agar plates supplemented with 30 μg/mL hygromycin for selection. Transforming DNA was a 1.7-kb gel-purified aph7″ expression cassette (Berthold et al., 2002) digested from plasmid pHyg3 with *Hind*III (New England Biolabs). After 4 to 5 d, colonies were picked into 96-well plates containing TAP, grown to saturation, and then pinned onto TAP and TAP + rapamycin plates. Rapamycin-hypersensitive mutants were identified by comparing growth on TAP versus TAP + 500 nM rapamycin. AZD8055 (LC Laboratories) and Torin1 (LC Laboratories) were used at 500 nM final concentration diluted from a 50 mM stock in DMSO.

Genetic Analysis

Gamete preparation, mating, and segregation analyses were done as described previously (Harris, 2009c). Random meiotic progeny isolated from among thousands of zygote colonies were individually grown in 96-well microtiter plates and pinned onto agar media plates supplemented with hygromycin or rapamycin. Mating type was scored using PCR genotyping (primers presented in Supplemental Table 1) (Zamora et al., 2004). Vegetative diploid strains (Ebersold, 1967) were generated using *vip1-1* and/or wild-type parental strains of the opposite mating type transformed with either a paromomycin resistance marker containing plasmid, pSI103 (Sizova et al., 2001) or a zeocin resistance marker containing plasmid, pSP124S (Lumbreras et al., 1998). Gametes of opposite mating type and containing different resistance markers were spread onto TAP agar containing 20 and 15 μg/mL zeocin shortly after mixing (1 to 2 h) and vegetative diploid colonies were picked and confirmed using PCR-based genotyping (Supplemental Table 1) (Zamora et al., 2004).

vip1-1 Mapping and Genotyping

Amplification of the pHYG3 insertion junction was performed according to a previously described strategy (O'Malley et al., 2007) using genomic DNA prepared as described (Umen and Goodenough, 2001). Genomic DNA from 266F3 was digested with *Pvu*II, *Sma*I, *Stu*I, and *Pml*I and blunt-end ligated to annealed adaptor oligonucleotides (Supplemental Table 1). Junction fragments were amplified using nested reactions with adaptor primers AP1 and AP2 along with IMPh5-1 and IMPh5-2, or with IMPh3-1 and IMPh3-2 (Supplemental Table 1). Cloned junction fragments were sequenced and the left border confirmed by amplifying and sequencing a 426-bp fragment amplified with IMPVIP3F and IMPVIP3R (Supplemental Figure 1 and Supplemental Table 1).

Genotyping was done using 0.5 μL of total genomic DNA prepared using a fast method described at http://www.chlamycollection.org/methods/quick-and-easy-genomic-dna-prep-for-pcr-analysis/. The *VIP1* wild-type allele was scored using VIPWTL and VIP1WTR (Supplemental Figure 1 and Supplemental Table 1), and the *vip1-1* allele was scored using VIPWTL and IMPVIPR. PCR was performed using Taq polymerase in a final reaction volume of 20 μL in the presence of 1× Taq buffer (Sambrook and Russell, 2001), 1 μM primers, 80 μM dNTP, 2% DMSO, and 0.5 μL of genomic DNA. PCR conditions were as follows: 96°C for 2 min and then 35 cycles of 94°C for 30 s, 60°C for 30 s, and 72°C for 30 s.

RNA extraction, cDNA synthesis, and RT-PCR were performed as previously described (Fang and Umen, 2008). VIP1WTL and VIP1WTR (Supplemental Figure 1 and Supplemental Table 1) were used to amplify cDNAs from the *VIP1* locus in the flanking region where pHYG is inserted in *vip1-1* (Supplemental Figure 1). PCR conditions were the same as above.

Cloning and Epitope Tagging of CrVIP1

Chlamydomonas BAC clone 4C23 (Kim et al., 1996) (http://www.genome.clemson.edu) was digested with *Psi*I and *Eco*RI and a 14628-bp fragment containing *VIP1* was gel purified. The *VIP1* fragment was ligated to pSI103 (Sizova et al., 2001) digested with *Sma*I and *Eco*RI to generate pVIP1. An OLLAS epitope (Park et al., 2008) was inserted into the N terminus of pVIP1 as follows. Two fragments (A and B) were amplified from *VIP1*, fragment A with primers OLLVIP1F and OLLVIP1R, and fragment B with primers OLLVIP2F and OLLVIP2R (Supplemental Table 1). OLLVIP1R and OLLVIP2F share an overlapping sequence that encodes the OLLAS tag sequence (Supplemental Table 1, underlined) and homology with *VIP1*. Both fragments were amplified using Taq polymerase as described above. pVIP1 and fragments A and B were digested with *Pfo*I (Thermo Scientific) (Supplemental Table 1, lowercase) and recombined using an In-Fusion HD Cloning Kit (Clontech) according to the manufacturer's instructions to generate pOLLAS-VIP1.

Complementation of *vip1-1*

vip1-1 was transformed by electroporation as described above and colonies were selected on TAP plates containing 30 μg/mL paromomycin. Transformants were picked and grown in 96-well plates in TAP until growth saturation and then they were pinned onto TAP containing 500 nM rapamycin. Positive clones were identified by loss of rapamycin

hypersensitivity with growth rates comparable to wild-type strains on rapamycin-containing plates. Complementation rates were calculated after testing paromomycin resistant colonies in rapamycin-containing media. Complementation rates were 15/480 for pOL-VIP1 and 2/80 for pVIP1.

Immunoblotting OLLAS-VIP

Protein extraction and immunoblotting to detect pOLLAS-VIP1 were performed as described previously (Olson et al., 2010) with the following modifications. Total protein loaded per well was 40 μg; rat α-OLLAS antibodies (NBP1-06713; Novus Biologicals; Lot A) were used at 1:1000 and HRP-conjugated secondary α-rat antibodies (Thermo Fisher Scientific; 31470) were used at 1:4000.

InsP Extraction and Analysis

The method described below allows separation and relative quantitation of InsP mass isomers $InsP_3$, $InsP_4$, $InsP_5$, $InsP_6$, $InsP_7$, and $InsP_8$. We cannot currently differentiate between InsP stereoisomers, but methodology to do so using mass spectrometry is under development. For InsP extraction, 300 mL of mid-log phase culture per sample was collected at a cell density of $\sim 2 \times 10^6$ cells/mL. (Cell density) × (mean cell size) measured using a Beckman-Coulter Multisizer3 was used as a metric for wet biomass. Sample volumes were adjusted slightly where necessary so that all replicates had identical wet biomasses. After harvesting by centrifugation (4000 rcf, 5 min, room temperature), cell pellets were resuspended in 1 mL final volume 5% trichloroacetic acid to extract InsPs and flash frozen in liquid nitrogen. After thawing, the samples were centrifuged at maximum speed for 20 min in a microfuge at 4°C. Each supernatant was then supplemented with 100 μL of 1 μM 3-fluoro-$InsP_3$ (3-deoxy-3-fluoro-D-myo-inositol 1,4,5-trisphosphate) (Enzo Life Sciences), which served as an internal standard for normalization. Supernatants were extracted three times with 2 mL of water-saturated diethyl ether. The pooled aqueous phase from the extractions was loaded onto a Strata-X AW column (Phenomenex; 30 mg resin; weak anion mixed mode phase 33-μm particle size). The column was washed with 1 mL of 25% methanol to remove trichloroacetic acid and other contaminants and the InsP were eluted using 1 mL of 100 mM ammonium carbonate. Then, 0.5 mL of acetic acid was added to each eluate and the samples were vacuum-dried. Each sample was resuspended in 50 μL of ultrapure water just prior to LC-MS/MS analysis. The final LC-MS/MS injection volume was 8 μL.

LC-MS/MS data were acquired using a Q-Exactive mass spectrometer (Thermo Fisher Scientific) equipped with a 1200 Capillary LC system (Agilent) and a 0.5 × 150-mm 5-μm BioBasic AX Column (Thermo Fisher Scientific) using chromatographic conditions adapted from Liu et al. (2009). The solvents were 250 mM ammonium carbonate (A) and 25% methanol (B). The gradient consisted of a hold for 4 min at 100% B, then a ramp to 10% A over 6 min, then up to 60% A in 7 min, and finally a ramp to 100% A over 3 min, followed by a hold at 100%A for 4 min. The solvent composition was returned to 100% B over 6 min and the column was reequilibrated for 40 min for a total per sample run time of 70 min. Mass spectrometric data were collected in negative ion profile mode at a resolution of 70,000 (at *m/z* 200) with a full scan from *m/z* 190 to 850 and SIM scans of 483.9 to 513.9, 563.9 to 593.9, 643.9 to 673.9, 723.9 to 753.8, and 803.9 to 833.8. Data were analyzed using the QualBrowser and QuanBrowser applications of Xcalibur (Thermo Fisher Scientific). Data were normalized using the internal standard 3-fluoro-$InsP_3$. Mean data and SD were calculated from three biological replicates, each of which had three technical replicates.

Metabolite Analysis

Mid-log phase ($\sim 2 \times 10^6$ mL^{-1}) cultures were harvested by fast vacuum filtering onto 50-mm Whatman filter paper (GE Healthcare Life Sciences; 1822-050), which was immediately quenched in liquid nitrogen with the total processing time for each sample kept under 10 s. Fresh weight (FW) for each sample was calculated by determining wet biomass volume (culture density × mean cell size × volume harvested). Packed cells have a density close to 1 mg/mL; therefore, FW in milligrams was equivalent to pellet volume in milliliters. Polar metabolites in frozen samples (5 to 8 mg FW) were extracted with methanol/chloroform/water (7:3:5.6) and analyzed via LC-MS/MS as previously described (Ma et al., 2014) with 0.3 nmole PIPES added to each sample as an internal standard. Metabolite concentrations (nmol gFW^{-1}) were determined by interpolating from the linear relationship between peak area and the concentrations of standards.

Lipid Analysis

Gas Chromatography-Flame Ionization Detection

Total lipid extraction and fatty acid methyl esters (FAMEs) were obtained from 5 mg of Chlamydomonas freeze-dried pellets using the method reported in Han et al. (2010) and using triheptadecanoin (C17:0 TAG) as an internal standard (Nu-Chek Prep). After evaporation under nitrogen gas, the samples were resuspended in 200 μL hexane and 1 μL was separated by Trace-GC with an FID detector (Thermo Fisher Scientific) fitted with an HP-INNOWax column (0.25-mm inner diameter and 30-m length) (Agilent). The oven temperature was programmed to 100°C (hold 1 min) to 235°C (hold 5 min) in a first ramp of 40°C/min until 185°C and then a second ramp of 7.5°C/min to 235°C. Peak assignments were made using FAME mix C8-C22 (Supelco) and the double-bond positions of the polyunsaturated fatty acids were confirmed by gas chromatography-mass spectrometry (Cahoon et al., 2006).

TLC

Twenty milligrams of freeze-dried pellet was used for extraction of total lipids using a modification of the standard Bligh and Dyer method (Bligh and Dyer, 1959). Four milliliters of $CHCl_3$:methanol (2:1) was added to the sample that was then mixed by vortexing. The samples were heated at 42°C for 30 min followed by addition of 2.5 mL 0.1 N HCL:1 M NaCl and additional mixing by vortexing. Samples were centrifuged for 2 min at 500 rcf at room temperature and then the aqueous (upper) phase was discarded. The organic phase was washed twice with ultrapure water and then dried under nitrogen gas. Samples were resuspended in 1 mL hexane and split into three equal (333 μL) parts. One part was transmethylated to FAMEs and analyzed by gas chromatography-flame ionization detection (GC-FID) as described above. A second part was used for TLC separation as described by Han et al. (2010) with image acquisition using an Alphaimager 2200 (AlphaInnotec). A mixture of standards was prepared using 18:1 free fatty acid, 18:1 triacylglycerol (TAG), 16:0/18:1 diacylglycerol, and 18:1 monoacylglycerol, 30 μg each, in 200 μL hexane. The third part was used for TAG separation on a silicic acid column with Iatrobeads of 0.5-cm internal diameter (Mitsubishi Kagaku Iatron). Columns were prepared using disposable glass Pasteur pipettes stopped with untreated glass wool and exactly 2 cm of beads. Columns were equilibrated with 4 mL hexane and then 200 μL of sample was loaded onto the column and TAGs were eluted with 4 mL of chloroform. Galactolipids and phospholipids were then eluted using 4 mL of acetane and methanol, respectively. After elution, all the fractions were dried and redissolved in hexane followed by fractionation on TLC plates or analysis by GC-FID, as described above.

Starch Analysis

Starch was measured using a Total Starch Assay Kit (AA/AMG; Megazyme) following the manufacturer's instructions, but scaled down to 10 mg freeze-dried cell powder as starting material. Mean and SD were calculated

from at least three biological replicates with three technical replicates per sample.

Fluorescence Microscopy

Nile Red Staining

Lipid body staining was performed as described (Wang et al., 2009). Microscopy was performed with a Leica DMI6000B using a 63× oil immersion objective with differential interference contrast (DIC) optics or wide-field fluorescence collected using a Leica L5 filter cube (excitation BP 480/40; dichroic 505; emission BP 527/30).

Immunofluorescence

Immunofluorescence was performed as described previously (Olson et al., 2010) with the following modifications. Primary rat α-OLLAS antibody (NBP1-06713, Lot A; Novus Biologicals) was used at 1:100 and secondary α-mouse (Alexa Fluor 488, A-11001, Lot 99C2-2; Thermo Fisher Scientific) was used at 1:1000, as recommended by the manufacturer. Microscopy was performed with a Leica DMI6000B using a 100× oil objective lens with DIC optics or using the following filter cube sets A4: excitation BP 360/40; dichroic 400; emission BP470/40, L5: excitation BP 480/40; dichroic 505; emission BP 527/30. Z stacks through the entire cell were collected for each image (20 × 0.2 μm).

Phylogenetic Tree Construction

Accession numbers for VIP1 homolog protein sequences used for alignment and tree construction are listed below. MEGA (Tamura et al., 2013) was used for all tree building steps. Sequences were aligned using MUSCLE (Edgar, 2004). All positions containing gaps and missing data were removed and an unrooted neighbor-joining tree was constructed using the JTT distance model with gamma set to 0.8 and 1000 bootstrap replicates.

Accession Numbers

Sequence data from this article can be found for Chlamydomonas genes in Phytozome (https://phytozome.jgi.doe.gov/pz/portal.html) under the following gene IDs: *FKB1*, Cre13.g586300; *CrVIP1*, Cre03.g185500; *CrVIP2*, Cre01.g052650; *CrITPK1*, Cre03.g182100; *CrITPK2*, Cre01.g018400; *CrIPMK*, Cre12.g555450; *CrIP5-2K*, Cre04.g229000; and *CrDIPP*, Cre02.g106500. The remaining sequences can be found at NCBI Protein database or GenBank (http://www.ncbi.nlm.nih.gov). Protein database accession numbers are as follows: *Volvox carteri* VcVIP1: XP_002948572.1, VcVIP2 XP_002946745.1, *Coccomyxa subellipsoidea* CsVIP1: XP_005644985.1; *Micromonas pusilla* MpVIP1: XP_003058868.1; *Ostreococcus tauri* OtVIP1; XP_003078214.1, *Ostreococcus lucimarinus* OlVIP1: XP_001416675; *Oryza sativa* OsVIP2: NP_001050945; *Arabidopsis thaliana* AtVIP1: NP_186780.3 and AtVip2: NP_001190313.1; *Homo sapiens* HsVIP1: NP_001124330.1 and HsVIP2: NP_001263206; *Thalassiosira pseudonana* CCMP1335 TpVIP1: XP_002288041.1; *Phaeodactylum tricornutum* CCAP 1055/1 PtVIP1: XP_002185836.1; *Ustilago maydis* UmVIP1: XP_011392692.1; *Aspergillus nidulans* FGSC A4 AnVIP1: XP_663401.1; *Caenorhabditis elegans* CeVIP1: NP_740855.2; *Schizosacharomyces pombe* SpVIP1: NP_587877.1; *Saccharomyces cerevisiae* ScVIP1: NP_013514; GenBank: *Oryza sativa* OsVIP1: EEE55479.1; *Drosophila melanogaster* DmVIP1: AAT94524.1.

Supplemental Data

Supplemental Figure 1. *vip1-1* insertion structure, genotyping, and dominance testing.

Supplemental Table 1. Sequence of primers used for mapping and genotyping *VIP1* or *vip1-1* and for constructing pOL-VIP1.

Supplemental Data Set 1. Alignment used to generate the phylogeny presented in Figure 2B.

ACKNOWLEDGMENTS

We thank Garrett Anderson for initial research design, initiation of the mutant screen, and identification of the insertion in *vip1-1*. We thank Thao Dang for assistance with the screen. We thank Marina Wantanabe, Wanda Waizenegger, Tuya Wulan, Fuqin Sun, Richard Davenport, and Thomas Connell for laboratory support. We thank Jan Jaworski for his suggestions and support on lipid quantitation and TAG separation and J.L. Crespo for kindly providing ATG8 antibodies and his suggestions for the interpretation of the results. The project was supported by the Center for Advanced Biofuel Systems, an Energy Frontier Research Center funded by the U.S. Department of Energy, Office of Basic Energy Sciences (DE-SC0001295), by the Department of Energy (DE-AR0000202), and by the National Science Foundation (DBI-1427621 and DBI-0521250).

AUTHOR CONTRIBUTIONS

J.G.U. and I.C. designed the research approach. J.G.U., I.C., and S.D. performed initial phenotypic analyses for carbon source effects and storage lipid phenotypes. J.G.U., I.C., and B.S.E. developed the methodology for analyzing inositol polyphosphates. I.C. and J.L. performed lipids analysis. I.C., Y.L., F.M., and D.K.A. collected and analyzed metabolite data. J.G.U. and I.C. wrote the article.

Received May 3, 2016; revised August 19, 2016; accepted September 2, 2016; published September 6, 2016.

REFERENCES

Azevedo, C., and Saiardi, A. (2006). Extraction and analysis of soluble inositol polyphosphates from yeast. Nat. Protoc. **1:** 2416–2422.

Barker, C.J., Illies, C., Gaboardi, G.C., and Berggren, P.O. (2009). Inositol pyrophosphates: structure, enzymology and function. Cell. Mol. Life Sci. **66:** 3851–3871.

Bennett, M., Onnebo, S.M.N., Azevedo, C., and Saiardi, A. (2006). Inositol pyrophosphates: metabolism and signaling. Cell. Mol. Life Sci. **63:** 552–564.

Berthold, P., Schmitt, R., and Mages, W. (2002). An engineered *Streptomyces hygroscopicus* aph 7" gene mediates dominant resistance against hygromycin B in *Chlamydomonas reinhardtii*. Protist **153:** 401–412.

Blaby, I.K., et al. (2013). Systems-level analysis of nitrogen starvation-induced modifications of carbon metabolism in a *Chlamydomonas reinhardtii* starchless mutant. Plant Cell **25:** 4305–4323.

Bligh, E.G., and Dyer, W.J. (1959). A rapid method of total lipid extraction and purification. Can. J. Biochem. Physiol. **37:** 911–917.

Boyle, N.R., et al. (2012). Three acyltransferases and nitrogen-responsive regulator are implicated in nitrogen starvation-induced triacylglycerol accumulation in Chlamydomonas. J. Biol. Chem. **287:** 15811–15825.

Boyle, N.R., and Morgan, J.A. (2009). Flux balance analysis of primary metabolism in *Chlamydomonas reinhardtii*. BMC Syst. Biol. **3:** 4.

Brown, E.J., Albers, M.W., Shin, T.B., Ichikawa, K., Keith, C.T., Lane, W.S., and Schreiber, S.L. (1994). A mammalian protein targeted by G1-arresting rapamycin-receptor complex. Nature **369:** 756–758.

Cahoon, E.B., Dietrich, C.R., Meyer, K., Damude, H.G., Dyer, J.M., and Kinney, A.J. (2006). Conjugated fatty acids accumulate to high levels in phospholipids of metabolically engineered soybean and Arabidopsis seeds. Phytochemistry **67:** 1166–1176.

Caldana, C., Li, Y., Leisse, A., Zhang, Y., Bartholomaeus, L., Fernie, A.R., Willmitzer, L., and Giavalisco, P. (2013). Systemic analysis of inducible target of rapamycin mutants reveal a general metabolic switch controlling growth in *Arabidopsis thaliana*. Plant J. **73:** 897–909.

Chakraborty, A., et al. (2010). Inositol pyrophosphates inhibit Akt signaling, thereby regulating insulin sensitivity and weight gain. Cell **143:** 897–910.

Chapman, S.P., Paget, C.M., Johnson, G.N., and Schwartz, J.-M. (2015). Flux balance analysis reveals acetate metabolism modulates cyclic electron flow and alternative glycolytic pathways in *Chlamydomonas reinhardtii*. Front. Plant Sci. **6:** 474.

Chresta, C.M., et al. (2010). AZD8055 is a potent, selective, and orally bioavailable ATP-competitive mammalian target of rapamycin kinase inhibitor with in vitro and in vivo antitumor activity. Cancer Res. **70:** 288–298.

Coruzzi, G., and Bush, D.R. (2001). Nitrogen and carbon nutrient and metabolite signaling in plants. Plant Physiol. **125:** 61–64.

Crespo, J.L., Díaz-Troya, S., and Florencio, F.J. (2005). Inhibition of target of rapamycin signaling by rapamycin in the unicellular green alga *Chlamydomonas reinhardtii*. Plant Physiol. **139:** 1736–1749.

Dent, R.M., Haglund, C.M., Chin, B.L., Kobayashi, M.C., and Niyogi, K.K. (2005). Functional genomics of eukaryotic photosynthesis using insertional mutagenesis of *Chlamydomonas reinhardtii*. Plant Physiol. **137:** 545–556.

Deprost, D., Yao, L., Sormani, R., Moreau, M., Leterreux, G., Nicolaï, M., Bedu, M., Robaglia, C., and Meyer, C. (2007). The Arabidopsis TOR kinase links plant growth, yield, stress resistance and mRNA translation. EMBO Rep. **8:** 864–870.

Desai, M., Rangarajan, P., Donahue, J.L., Williams, S.P., Land, E.S., Mandal, M.K., Phillippy, B.Q., Perera, I.Y., Raboy, V., and Gillaspy, G.E. (2014). Two inositol hexakisphosphate kinases drive inositol pyrophosphate synthesis in plants. Plant J. **80:** 642–653.

Díaz-Troya, S., Pérez-Pérez, M.E., Florencio, F.J., and Crespo, J.L. (2008). The role of TOR in autophagy regulation from yeast to plants and mammals. Autophagy **4:** 851–865.

Ebersold, W.T. (1967). *Chlamydomonas reinhardi*: heterozygous diploid strains. Science **157:** 447–449.

Edgar, R.C. (2004). MUSCLE: a multiple sequence alignment method with reduced time and space complexity. BMC Bioinformatics **5:** 113.

Fang, S.-C., and Umen, J.G. (2008). A suppressor screen in chlamydomonas identifies novel components of the retinoblastoma tumor suppressor pathway. Genetics **178:** 1295–1310.

Fridy, P.C., Otto, J.C., Dollins, D.E., and York, J.D. (2007). Cloning and characterization of two human VIP1-like inositol hexakisphosphate and diphosphoinositol pentakisphosphate kinases. J. Biol. Chem. **282:** 30754–30762.

Galván, A., González-Ballester, D., and Fernández, E. (2007). Insertional mutagenesis as a tool to study genes/functions in Chlamydomonas. Adv. Exp. Med. Biol. **616:** 77–89.

Gillaspy, G.E. (2011). The cellular language of myo-inositol signaling. New Phytol. **192:** 823–839.

Gillaspy, G.E. (2013). The role of phosphoinositides and inositol phosphates in plant cell signaling. Adv. Exp. Med. Biol. **991:** 141–157.

Gilliland, L.U., Magallanes-Lundback, M., Hemming, C., Supplee, A., Koornneef, M., Bentsink, L., and Dellapenna, D. (2006). Genetic basis for natural variation in seed vitamin E levels in *Arabidopsis thaliana*. Proc. Natl. Acad. Sci. USA **103:** 18834–18841.

Giroud, C., Gerber, A., and Eichenberger, W. (1988). Lipids of *Chlamydomonas reinhardtii*. Analysis of molecular species and intracellular site(s) of biosynthesis. Plant Cell Physiol. **29:** 587–595.

Goodenough, U. (2015). Historical perspective on Chlamydomonas as a model for basic research: 1950-1970. Plant J. **82:** 365–369.

Goodenough, U., et al. (2014). The path to triacylglyceride obesity in the sta6 strain of *Chlamydomonas reinhardtii*. Eukaryot. Cell **13:** 591–613.

Grossman, A.R. (2000). *Chlamydomonas reinhardtii* and photosynthesis: genetics to genomics. Curr. Opin. Plant Biol. **3:** 132–137.

Halford, N.G., and Paul, M.J. (2003). Carbon metabolite sensing and signalling. Plant Biotechnol. J. **1:** 381–398.

Han, J., Clement, J.M., Li, J., King, A., Ng, S., and Jaworski, J.G. (2010). The cytochrome P450 CYP86A22 is a fatty acyl-CoA omega-hydroxylase essential for Estolide synthesis in the stigma of *Petunia hybrida*. J. Biol. Chem. **285:** 3986–3996.

Harris, E.H. (2009a). Chlamydomonas in the laboratory. In The Chlamydomonas Sourcebook, E.H. Harris, D.B. Stern, and G.B. Witman, eds (Burlington, MA: Elsevier), pp. 241–302.

Harris, E.H. (2009b). The life of an acetate flagellate. In The Chlamydomonas Sourcebook, E.H. Harris, D.B. Stern, and G.B. Witman, eds (Burlington, MA: Elsevier), pp. 159–210.

Harris, E.H. (2009c). The Sexual Cycle. In The Chlamydomonas Sourcebook, E.H. Harris, D.B. Stern, and G.B. Witman, eds (Burlington, MA: Elsevier), pp. 119–157.

Heifetz, P.B., Fo, B., Osmond, C.B., Giles, L.J., and Boynton, J.E. (2000). Effects of acetate on facultative autotrophy in *Chlamydomonas reinhardtii* assessed by photosynthetic measurements and stable isotope analyses. Plant Physiol. **122:** 1439–1445.

Heitman, J., Movva, N.R., and Hall, M.N. (1991). Targets for cell cycle arrest by the immunosuppressant rapamycin in yeast. Science **253:** 905–909.

Hu, Q., Sommerfeld, M., Jarvis, E., Ghirardi, M., Posewitz, M., Seibert, M., and Darzins, A. (2008). Microalgal triacylglycerols as feedstocks for biofuel production: perspectives and advances. Plant J. **54:** 621–639.

Im, C.S., and Beale, S.I. (2000). Identification of possible signal transduction components mediating light induction of the Gsa gene for an early chlorophyll biosynthetic step in *Chlamydomonas reinhardtii*. Planta **210:** 999–1005.

Irvine, R.F., Letcher, A.J., Stephens, L.R., and Musgrave, A. (1992). Inositol polyphosphate metabolism and inositol lipids in a green alga, *Chlamydomonas eugametos*. Biochem. J. **281:** 261–266.

Irvine, R.F., and Schell, M.J. (2001). Back in the water: the return of the inositol phosphates. Nat. Rev. Mol. Cell Biol. **2:** 327–338.

Johnson, X., and Alric, J. (2012). Interaction between starch breakdown, acetate assimilation, and photosynthetic cyclic electron flow in *Chlamydomonas reinhardtii*. J. Biol. Chem. **287:** 26445–26452.

Kajikawa, M., Sawaragi, Y., Shinkawa, H., Yamano, T., Ando, A., Kato, M., Hirono, M., Sato, N., and Fukuzawa, H. (2015). Algal dual-specificity tyrosine phosphorylation-regulated kinase, triacylglycerol accumulation regulator1, regulates accumulation of triacylglycerol in nitrogen or sulfur deficiency. Plant Physiol. **168:** 752–764.

Kim, J., and Guan, K.L. (2011). Amino acid signaling in TOR activation. Annu. Rev. Biochem. **80:** 1001–1032.

Kim, U.J., Birren, B.W., Slepak, T., Mancino, V., Boysen, C., Kang, H.L., Simon, M.I., and Shizuya, H. (1996). Construction and characterization of a human bacterial artificial chromosome library. Genomics **34:** 213–218.

Koch, K. (2004). Sucrose metabolism: regulatory mechanisms and pivotal roles in sugar sensing and plant development. Curr. Opin. Plant Biol. **7:** 235–246.

Laha, D. et al. (2015) VIH2 regulates the synthesis of inositol pyrophosphate InsP8 and jasmonate-dependent defenses in Arabidopsis. Plant Cell **27:** 1082–1097.

Li, X., Moellering, E.R., Liu, B., Johnny, C., Fedewa, M., Sears, B.B., Kuo, M.-H., and Benning, C. (2012). A galactoglycerolipid lipase is required for triacylglycerol accumulation and survival following nitrogen deprivation in *Chlamydomonas reinhardtii*. Plant Cell **24:** 4670–4686.

Li, Y., Han, D., Hu, G., Dauvillee, D., Sommerfeld, M., Ball, S., and Hu, Q. (2010a). Chlamydomonas starchless mutant defective in

ADP-glucose pyrophosphorylase hyper-accumulates triacylglycerol. Metab. Eng. **12:** 387–391.

Li, Y., Han, D., Hu, G., Sommerfeld, M., and Hu, Q. (2010b). Inhibition of starch synthesis results in overproduction of lipids in *Chlamydomonas reinhardtii*. Biotechnol. Bioeng. **107:** 258–268.

Lin, H., Fridy, P.C., Ribeiro, A.A., Choi, J.H., Barma, D.K., Vogel, G., Falck, J.R., Shears, S.B., York, J.D., and Mayr, G.W. (2009). Structural analysis and detection of biological inositol pyrophosphates reveal that the family of VIP/diphosphoinositol pentakisphosphate kinases are 1/3-kinases. J. Biol. Chem. **284:** 1863–1872.

Liu, B., and Benning, C. (2013). Lipid metabolism in microalgae distinguishes itself. Curr. Opin. Biotechnol. **24:** 300–309.

Liu, X., Villalta, P.W., and Sturla, S.J. (2009). Simultaneous determination of inositol and inositol phosphates in complex biological matrices: quantitative ion-exchange chromatography/tandem mass spectrometry. Rapid Commun. Mass Spectrom. **23:** 705–712.

Liu, Y., and Bassham, D.C. (2010). TOR is a negative regulator of autophagy in *Arabidopsis thaliana*. PLoS One **5:** e11883.

Livermore, T.M., Azevedo, C., Kolozsvari, B., Wilson, M.S.C., and Saiardi, A. (2016). Phosphate, inositol and polyphosphates. Biochem. Soc. Trans. **44:** 253–259.

Loewith, R., and Hall, M.N. (2011). Target of rapamycin (TOR) in nutrient signaling and growth control. Genetics **189:** 1177–1201.

Loewus, F.A., and Murthy, P.P.N. (2000). myo-Inositol metabolism in plants. Plant Sci. **150:** 1–19.

Losito, O., Szijgyarto, Z., Resnick, A.C., and Saiardi, A. (2009). Inositol pyrophosphates and their unique metabolic complexity: analysis by gel electrophoresis. PLoS One **4:** e5580.

Lumbreras, V., Stevens, D.R., and Purton, S. (1998). Efficient foreign gene expression in Chlamydomonas reinhardtii mediated by an endogenous intron. Plant J. **14:** 441–447.

Ma, F., Jazmin, L.J., Young, J.D., and Allen, D.K. (2014). Isotopically nonstationary 13C flux analysis of changes in *Arabidopsis thaliana* leaf metabolism due to high light acclimation. Proc. Natl. Acad. Sci. USA **111:** 16967–16972.

Maegawa, K., Takii, R., Ushimaru, T., and Kozaki, A. (2015). Evolutionary conservation of TORC1 components, TOR, Raptor, and LST8, between rice and yeast. Mol. Genet. Genomics **290:** 2019–2030.

Markou, G., and Nerantzis, E. (2013). Microalgae for high-value compounds and biofuels production: a review with focus on cultivation under stress conditions. Biotechnol. Adv. **31:** 1532–1542.

Mayfield, S., and Golden, S.S. (2015). Photosynthetic biomanufacturing: food, fuel, and medicine for the 21st century. Photosynth. Res. **123:** 225–226.

Menand, B., Desnos, T., Nussaume, L., Berger, F., Bouchez, D., Meyer, C., and Robaglia, C. (2002). Expression and disruption of the Arabidopsis TOR (target of rapamycin) gene. Proc. Natl. Acad. Sci. USA **99:** 6422–6427.

Merchant, S.S., Kropat, J., Liu, B., Shaw, J., and Warakanont, J. (2012). TAG, you're it! Chlamydomonas as a reference organism for understanding algal triacylglycerol accumulation. Curr. Opin. Biotechnol. **23:** 352–363.

Miller, R., et al. (2010). Changes in transcript abundance in *Chlamydomonas reinhardtii* following nitrogen deprivation predict diversion of metabolism. Plant Physiol. **154:** 1737–1752.

Minagawa, J., and Tokutsu, R. (2015). Dynamic regulation of photosynthesis in *Chlamydomonas reinhardtii*. Plant J. **82:** 413–428.

Monserrate, J.P., and York, J.D. (2010). Inositol phosphate synthesis and the nuclear processes they affect. Curr. Opin. Cell Biol. **22:** 365–373.

Montané, M.-H., and Menand, B. (2013). ATP-competitive mTOR kinase inhibitors delay plant growth by triggering early differentiation of meristematic cells but no developmental patterning change. J. Exp. Bot. **64:** 4361–4374.

Morales-Sánchez, D., Martinez-Rodriguez, O.A., Kyndt, J., and Martinez, A. (2015). Heterotrophic growth of microalgae: metabolic aspects. World J. Microbiol. Biotechnol. **31:** 1–9.

Moreau, M., Azzopardi, M., Clément, G., Dobrenel, T., Marchive, C., Renne, C., Martin-Magniette, M.-L., Taconnat, L., Renou, J.-P., Robaglia, C., and Meyer, C. (2012). Mutations in the Arabidopsis homolog of LST8/GβL, a partner of the target of Rapamycin kinase, impair plant growth, flowering, and metabolic adaptation to long days. Plant Cell **24:** 463–481.

Mosblech, A., König, S., Stenzel, I., Grzeganek, P., Feussner, I., and Heilmann, I. (2008). Phosphoinositide and inositolpolyphosphate signalling in defense responses of *Arabidopsis thaliana* challenged by mechanical wounding. Mol. Plant **1:** 249–261.

Mosblech, A., Thurow, C., Gatz, C., Feussner, I., and Heilmann, I. (2011). Jasmonic acid perception by COI1 involves inositol polyphosphates in *Arabidopsis thaliana*. Plant J. **65:** 949–957.

Msanne, J., Xu, D., Konda, A.R., Casas-Mollano, J.A., Awada, T., Cahoon, E.B., and Cerutti, H. (2012). Metabolic and gene expression changes triggered by nitrogen deprivation in the photoautotrophically grown microalgae *Chlamydomonas reinhardtii* and Coccomyxa sp. C-169. Phytochemistry **75:** 50–59.

Mulugu, S., Bai, W., Fridy, P.C., Bastidas, R.J., Otto, J.C., Dollins, D.E., Haystead, T.A., Ribeiro, A.A., and York, J.D. (2007). A conserved family of enzymes that phosphorylate inositol hexakisphosphate. Science **316:** 106–109.

Munnik, T., Irvine, R., and Musgrave, A. (1998). Phospholipid signalling in plants. Biochim. Biophys. Acta **1389:** 222–272.

Nagata, E., Luo, H.R., Saiardi, A., Bae, B.I., Suzuki, N., and Snyder, S.H. (2005). Inositol hexakisphosphate kinase-2, a physiologic mediator of cell death. J. Biol. Chem. **280:** 1634–1640.

Ngan, C.Y., et al. (2015). Lineage-specific chromatin signatures reveal a regulator of lipid metabolism in microalgae. Nat. Plants **1:** 15107.

Olson, B.J.S.C., Oberholzer, M., Li, Y., Zones, J.M., Kohli, H.S., Bisova, K., Fang, S.-C., Meisenhelder, J., Hunter, T., and Umen, J.G. (2010). Regulation of the Chlamydomonas cell cycle by a stable, chromatin-associated retinoblastoma tumor suppressor complex. Plant Cell **22:** 3331–3347.

O'Malley, R.C., Alonso, J.M., Kim, C.J., Leisse, T.J., and Ecker, J.R. (2007). An adapter ligation-mediated PCR method for high-throughput mapping of T-DNA inserts in the Arabidopsis genome. Nat. Protoc. **2:** 2910–2917.

Park, S.H., Cheong, C., Idoyaga, J., Kim, J.Y., Choi, J.H., Do, Y., Lee, H., Jo, J.H., Oh, Y.S., Im, W., Steinman, R.M., and Park, C.G. (2008). Generation and application of new rat monoclonal antibodies against synthetic FLAG and OLLAS tags for improved immunodetection. J. Immunol. Methods **331:** 27–38.

Plancke, C., et al. (2014). Lack of isocitrate lyase in Chlamydomonas leads to changes in carbon metabolism and in the response to oxidative stress under mixotrophic growth. Plant J. **77:** 404–417.

Pöhlmann, J., Risse, C., Seidel, C., Pohlmann, T., Jakopec, V., Walla, E., Ramrath, P., Takeshita, N., Baumann, S., Feldbrügge, M., Fischer, R., and Fleig, U. (2014). The Vip1 inositol polyphosphate kinase family regulates polarized growth and modulates the microtubule cytoskeleton in fungi. PLoS Genet. **10:** e1004586.

Pringsheim, E.G., and Wiessner, W. (1960). Photo-assimilation of acetate by green organisms. Nature **188:** 919–921.

Pröschold, T., Marin, B., Schlösser, U.G., and Melkonian, M. (2001). Molecular phylogeny and taxonomic revision of Chlamydomonas (Chlorophyta). I. Emendation of *Chlamydomonas ehrenberg* and *Chloromonas gobi*, and description of Oogamochlamys gen. nov. and Lobochlamys gen. nov. Protist **152:** 265–300.

Quarmby, L.M., and Hartzell, H.C. (1994). Two distinct, calcium-mediated, signal transduction pathways can trigger deflagellation in *Chlamydomonas reinhardtii*. J. Cell Biol. **124:** 807–815.

Raboy, V. (2003). myo-Inositol-1,2,3,4,5,6-hexakisphosphate. Phytochemistry **64:** 1033–1043.

Ren, M., et al. (2012). Target of rapamycin signaling regulates metabolism, growth, and life span in Arabidopsis. Plant Cell **24:** 4850–4874.

Rexin, D., Meyer, C., Robaglia, C., and Veit, B. (2015). TOR signalling in plants. Biochem. J. **470:** 1–14.

Roach, T., Sedoud, A., and Krieger-Liszkay, A. (2013). Acetate in mixotrophic growth medium affects photosystem II in *Chlamydomonas reinhardtii* and protects against photoinhibition. Biochim. Biophys. Acta **1827:** 1183–1190.

Rochaix, J.D. (1995). *Chlamydomonas reinhardtii* as the photosynthetic yeast. Annu. Rev. Genet. **29:** 209–230.

Sabatini, D.M., Erdjument-Bromage, H., Lui, M., Tempst, P., and Snyder, S.H. (1994). RAFT1: a mammalian protein that binds to FKBP12 in a rapamycin-dependent fashion and is homologous to yeast TORs. Cell **78:** 35–43.

Sager, R. (1955). Inheritance in the green alga *Chlamydomonas reinhardi*. Genetics **40:** 476–489.

Saiardi, A. (2012). Cell signalling by inositol pyrophosphates. Subcell. Biochem. **59:** 413–443.

Sambrook, J., and Russell, D.W. (2001). Molecular Cloning: A Laboratory Manual, Vol. 1. (Cold Spring Harbor, NY: Cold Spring Harbor Laboratory Press).

Scranton, M.A., Ostrand, J.T., Fields, F.J., and Mayfield, S.P. (2015). Chlamydomonas as a model for biofuels and bio-products production. Plant J. **82:** 523–531.

Sheard, L.B., et al. (2010). Jasmonate perception by inositol-phosphate-potentiated COI1-JAZ co-receptor. Nature **468:** 400–405.

Shears, S.B. (2009). Diphosphoinositol polyphosphates: metabolic messengers? Mol. Pharmacol. **76:** 236–252.

Sheen, J. (1994). Feedback control of gene expression. Photosynth. Res. **39:** 427–438.

Shimogawara, K., Fujiwara, S., Grossman, A., and Usuda, H. (1998). High-efficiency transformation of *Chlamydomonas reinhardtii* by electroporation. Genetics **148:** 1821–1828.

Siaut, M., Cuiné, S., Cagnon, C., Fessler, B., Nguyen, M., Carrier, P., Beyly, A., Beisson, F., Triantaphylidès, C., Li-Beisson, Y., and Peltier, G. (2011). Oil accumulation in the model green alga *Chlamydomonas reinhardtii*: characterization, variability between common laboratory strains and relationship with starch reserves. BMC Biotechnol. **11:** 7.

Sizova, I., Fuhrmann, M., and Hegemann, P. (2001). A Streptomyces rimosus aphVIII gene coding for a new type phosphotransferase provides stable antibiotic resistance to *Chlamydomonas reinhardtii*. Gene **277:** 221–229.

Smith, A.M., and Stitt, M. (2007). Coordination of carbon supply and plant growth. Plant Cell Environ. **30:** 1126–1149.

Stevenson-Paulik, J., Chiou, S.-T., Frederick, J.P., dela Cruz, J., Seeds, A.M., Otto, J.C., and York, J.D. (2006). Inositol phosphate metabolomics: merging genetic perturbation with modernized radiolabeling methods. Methods **39:** 112–121.

Tamura, K., Stecher, G., Peterson, D., Filipski, A., and Kumar, S. (2013). MEGA6: Molecular Evolutionary Genetics Analysis version 6.0. Mol. Biol. Evol. **30:** 2725–2729.

Tan, X., Calderon-Villalobos, L.I., Sharon, M., Zheng, C., Robinson, C.V., Estelle, M., and Zheng, N. (2007). Mechanism of auxin perception by the TIR1 ubiquitin ligase. Nature **446:** 640–645.

Thoreen, C.C., Kang, S.A., Chang, J.W., Liu, Q., Zhang, J., Gao, Y., Reichling, L.J., Sim, T., Sabatini, D.M., and Gray, N.S. (2009). An ATP-competitive mammalian target of rapamycin inhibitor reveals rapamycin-resistant functions of mTORC1. J. Biol. Chem. **284:** 8023–8032.

Thota, S.G., and Bhandari, R. (2015). The emerging roles of inositol pyrophosphates in eukaryotic cell physiology. J. Biosci. **40:** 593–605.

Tsai, C.H., Warakanont, J., Takeuchi, T., Sears, B.B., Moellering, E.R., and Benning, C. (2014). The protein Compromised Hydrolysis of Triacylglycerols 7 (CHT7) acts as a repressor of cellular quiescence in Chlamydomonas. Proc. Natl. Acad. Sci. USA **111:** 15833–15838.

Tsui, M.M., and York, J.D. (2010). Roles of inositol phosphates and inositol pyrophosphates in development, cell signaling and nuclear processes. Adv. Enzyme Regul. **50:** 324–337.

Umen, J.G., and Goodenough, U.W. (2001). Chloroplast DNA methylation and inheritance in Chlamydomonas. Genes Dev. **15:** 2585–2597.

Vallon, O. (2005). Chlamydomonas immunophilins and parvulins: survey and critical assessment of gene models. Eukaryot. Cell **4:** 230–241.

Wang, Z.T., Ullrich, N., Joo, S., Waffenschmidt, S., and Goodenough, U. (2009). Algal lipid bodies: stress induction, purification, and biochemical characterization in wild-type and starchless *Chlamydomonas reinhardtii*. Eukaryot. Cell **8:** 1856–1868.

Wase, N., Black, P.N., Stanley, B.A., and DiRusso, C.C. (2014). Integrated quantitative analysis of nitrogen stress response in *Chlamydomonas reinhardtii* using metabolite and protein profiling. J. Proteome Res. **13:** 1373–1396.

Wild, R., Gerasimaite, R., Jung, J.-Y., Truffault, V., Pavlovic, I., Schmidt, A., Saiardi, A., Jessen, H.J., Poirier, Y., Hothorn, M., and Mayer, A. (2016). Control of eukaryotic phosphate homeostasis by inositol polyphosphate sensor domains. Science **352:** 986–990.

Williams, S.P., Gillaspy, G.E., and Perera, I.Y. (2015). Biosynthesis and possible functions of inositol pyrophosphates in plants. Front. Plant Sci. **6:** 67.

Wilson, M.S.C., Livermore, T.M., and Saiardi, A. (2013). Inositol pyrophosphates: between signalling and metabolism. Biochem. J. **452:** 369–379.

Work, V.H., Radakovits, R., Jinkerson, R.E., Meuser, J.E., Elliott, L.G., Vinyard, D.J., Laurens, L.M.L., Dismukes, G.C., and Posewitz, M.C. (2010). Increased lipid accumulation in the *Chlamydomonas reinhardtii sta7-10* starchless isoamylase mutant and increased carbohydrate synthesis in complemented strains. Eukaryot. Cell **9:** 1251–1261.

Worley, J., Luo, X., and Capaldi, A.P. (2013). Inositol pyrophosphates regulate cell growth and the environmental stress response by activating the HDAC Rpd3L. Cell Reports **3:** 1476–1482.

Wundenberg, T., and Mayr, G.W. (2012). Synthesis and biological actions of diphosphoinositol phosphates (inositol pyrophosphates), regulators of cell homeostasis. Biol. Chem. **393:** 979–998.

Xie, B., Stessman, D., Hart, J.H., Dong, H., Wang, Y., Wright, D.A., Nikolau, B.J., Spalding, M.H., and Halverson, L.J. (2014). High-throughput fluorescence-activated cell sorting for lipid hyperaccumulating *Chlamydomonas reinhardtii* mutants. Plant Biotechnol. J. **12:** 872–882.

Xiong, Y., McCormack, M., Li, L., Hall, Q., Xiang, C., and Sheen, J. (2013). Glucose-TOR signalling reprograms the transcriptome and activates meristems. Nature **496:** 181–186.

Xiong, Y., and Sheen, J. (2015). Novel links in the plant TOR kinase signaling network. Curr. Opin. Plant Biol. **28:** 83–91.

Xiong, Y., and Sheen, J. (2012). Rapamycin and glucose-target of rapamycin (TOR) protein signaling in plants. J. Biol. Chem. **287:** 2836–2842.

Yueh, Y.G., and Crain, R.C. (1993). Deflagellation of *Chlamydomonas reinhardtii* follows a rapid transitory accumulation of inositol 1,4,5-trisphosphate and requires Ca^{2+} entry. J. Cell Biol. **123:** 869–875.

Zamora, I., Feldman, J.L., and Marshall, W.F. (2004). PCR-based assay for mating type and diploidy in Chlamydomonas. Biotechniques **37:** 534–536.

Zones, J.M., Blaby, I.K., Merchant, S.S., and Umen, J.G. (2015). High-resolution profiling of a synchronized diurnal transcriptome from *Chlamydomonas reinhardtii* reveals continuous cell and metabolic differentiation. Plant Cell **27:** 2743–2769.